AD-A162 111 COMBUSTOR/INLET INTERACTIONS AND MODELING OF HYPERSONIC DUAL COMBUSTOR RA (U) JOHNS HOPKINS UNIV LAUREL MD APPLIED PHYSICS LAB R D STOCKBRIDGE ET AL 19 NOV 84 1/1

UNCLASSIFIED AFOSR-TR-85-1063 AFOSR-MIPR-84-00001 F/G 21/2 NL

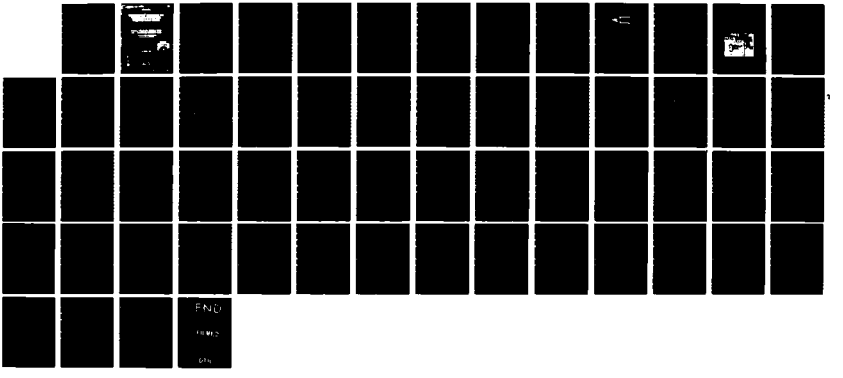

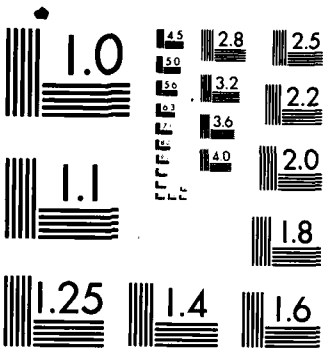

MICROCOPY RESOLUTION TEST CHART
NATIONAL BUREAU OF STANDARDS-1963-A

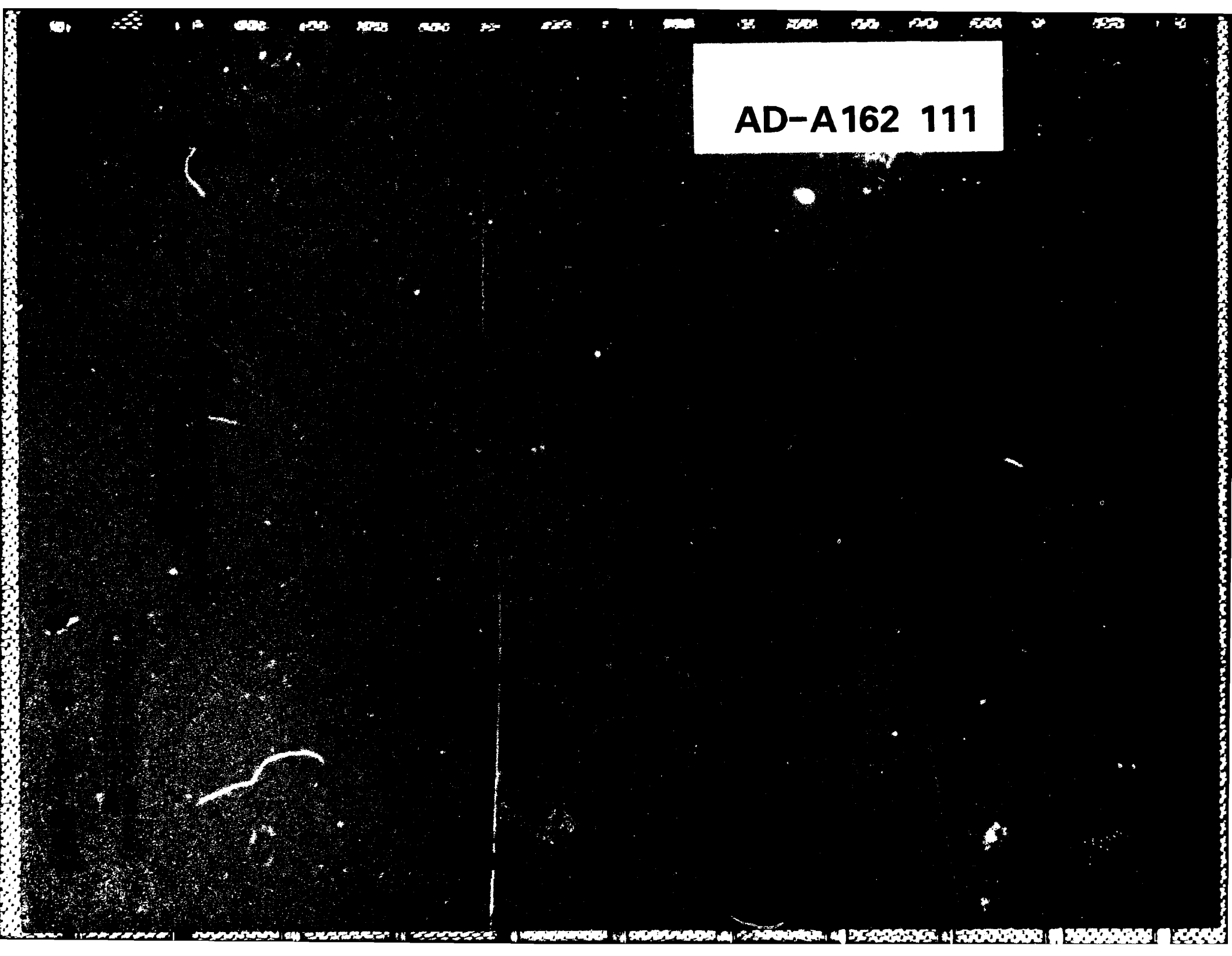

UNCLASSIFIED

SECURITY CLASSIFICATION OF THIS PAGE

REPORT DOCUMENTATION PAGE

1a. REPORT SECURITY CLASSIFICATION UNCLASSIFIED	1b. RESTRICTIVE MARKINGS
2a. SECURITY CLASSIFICATION AUTHORITY	3 DISTRIBUTION / AVAILABILITY OF REPORT Approved for public release; distribution unlimited.
2b. DECLASSIFICATION / DOWNGRADING SCHEDULE	
4. PERFORMING ORGANIZATION REPORT NUMBER(S) AFOSR-TR-84	5. MONITORING ORGANIZATION REPORT NUMBER(S) AFOSR-TR- 85-1063
6a. NAME OF PERFORMING ORGANIZATION Johns Hopkins University/ Applied Physics Laboratory 6b. OFFICE SYMBOL (If applicable)	7a. NAME OF MONITORING ORGANIZATION AFOSR/NA
6c. ADDRESS (City, State, and ZIP Code) Johns Hopkins Road Laurel, MD 20707	7b. ADDRESS (City, State, and ZIP Code) Bolling AFB DC 20332-6448
8a. NAME OF FUNDING / SPONSORING ORGANIZATION AFOSR/NA 8b. OFFICE SYMBOL (If applicable) AFOSR/NA	9. PROCUREMENT INSTRUMENT IDENTIFICATION NUMBER AFOSR-MIPR-84-00001
8c. ADDRESS (City, State, and ZIP Code) Bldg. 410 - Room 223 Bolling AFB, Washington, DC 20332-6448	10. SOURCE OF FUNDING NUMBERS PROGRAM ELEMENT NO. 61102F; PROJECT NO. 2308; TASK NO. A2; WORK UNIT ACCESSION NO.

11. TITLE (Include Security Classification)

Combustor/Inlet Interactions and Modeling of Hypersonic Dual Combustion Ramjet Engines

12. PERSONAL AUTHOR(S)

Richard D. Stockbridge, Joseph A. Schetz, Paul J. Waltrup and Frederick S. Billig

13a. TYPE OF REPORT	13b. TIME COVERED	14. DATE OF REPORT (Year, Month, Day)	15. PAGE COUNT
FINAL	FROM 10/83 TO 9/84	1984 November 19	54

16. SUPPLEMENTARY NOTATION

17. COSATI CODES			18. SUBJECT TERMS (Continue on reverse if necessary and identify by block number)
FIELD	GROUP	SUB-GROUP	Combustor/Inlet Interactions; Mixing and Combustion; Shock Boundary Layer Interactions; Supersonic Combustion. Skin Friction and Heat Transfer;

19. ABSTRACT (Continue on reverse if necessary and identify by block number)

This final report documents the accomplishments and status of the Dual Combustion Ramjet (DCR) research project as of September 30, 1984. The purpose of this research has been to experimentally and analytically describe the inlet/combustor/exit nozzle flowfields in hypersonic DCR engines. The experimental effort to date describes, in part, the flow characteristics in the isolator duct that conducts air supersonically from the external flowfield of the hypersonic air inlet to the supersonic combustor. This description includes the mean flow properties, the turbulent fluctuation flow properties, the boundary layer growth and the simulated precombustion compression field for an initial Mach 2.4 flow in a 20-in. long annular duct with inner and outer radii of 3.125 and 4.2 in., respectively. The analytical effort includes models that describe: (1) the recirculation region at the DCR gas generator base created by a surrounding supersonic jet; (2) the mixing and burning processes in the DCR supersonic combustor; (3) the supersonic combustor boundary layer; and (4) the nozzle flow. The models include such enhancements as finite rate, multiple species

20. DISTRIBUTION / AVAILABILITY OF ABSTRACT ☒ UNCLASSIFIED/UNLIMITED ☐ SAME AS RPT. ☐ DTIC USERS	21. ABSTRACT SECURITY CLASSIFICATION UNCLASSIFIED
22a. NAME OF RESPONSIBLE INDIVIDUAL Dr. Julian Tishkoff	22b. TELEPHONE (Include Area Code) 202/767-4935 22c. OFFICE SYMBOL AFOSR/NA

DD FORM 1473, 84 MAR

83 APR edition may be used until exhausted.
All other editions are obsolete.

SECURITY CLASSIFICATION OF THIS PAGE

UNCLASSIFIED

19. chemistry, the solution of the full Navier-Stokes equations for axisymmetric flow and energy transfer due to mass diffusion.

AFOSR-TR-84-

COMBUSTOR/INLET INTERACTIONS AND MODELING OF HYPERSONIC DUAL COMBUSTOR RAMJET ENGINES

RICHARD D. STOCKBRIDGE, JOSEPH A. SCHETZ,
PAUL J. WALTRUP AND FREDERICK S. BILLIG

The Johns Hopkins University/Applied Physics Laboratory
Johns Hopkins Road, Laurel, MD 20707

OCTOBER 1984

AIR FORCE OFFICE OF SCIENTIFIC RESEARCH
Bolling Air Force Base
Washington, DC 20332

CONTENTS

FIGURES

TABLES

TABLES (continued)

APPENDIX

HYPERSONIC DUAL COMBUSTION RAMJET ENGINES

Richard D. Stockbridge, Joseph A. Schetz, Paul J. Waltrup,
and Frederick S. Billig

The Johns Hopkins University Applied Physics Laboratory
Laurel, Maryland 20707

INTRODUCTION

Requirements for future offensive and defensive weapon systems necessitate the development of long range, very high speed missiles to effectively counter the continually improving capabilities of potentially hostile nations. Of the candidate propulsion cycles available to power these missiles, only rockets and advanced ramjets employing supersonic combustion as their primary mode of combustion are capable of providing the hypersonic speeds required. However, rockets must fly exo-atmospheric trajectories to achieve the needed ranges, and since they are coasting after reentry, their ability to make corrections and to intercept maneuvering targets is limited. On the other hand, advanced hypersonic ramjets, which remain within the atmosphere, are capable of sustained powered flight, including course changes and interception of maneuvering targets.

These clear advantages of an advanced hypersonic airbreathing propulsion system establish the need to develop a basic knowledge and understanding of the overall engine cycle, individual component flowfields and engine thermochemistry in hypersonic dual-combustion ramjet engines. This goal is being pursued by both an analytical approach and by an experimental approach that focus on different aspects of this problem. The analytical approach involves the development of theoretical models that describe the dual-combustion process with empnasis on the supersonic combustor and exit nozzle. The experimental approach is being used to establish a sound data base and a corresponding semi-empirical model applicable over the range of simulated flight conditions that will describe the interaction of the compression field generated at the entrance of supersonic combustors with the exit flowfield of hypersonic air inlets.

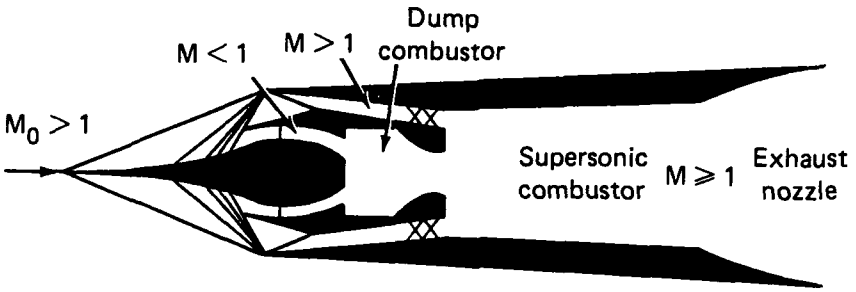

Fig. 1 Schematic of dual combustion ramjet engine.

Fig. 1 is a schematic diagram of the Dual Combustion Ramjet (DCR) engine concept. The freestream air is initially compressed by an external inlet diffuser. The inner cowl lip then subdivides the compressed air, and a small portion is ducted to a small, dump-type subsonic combustor. All of the fuel is added in the subsonic combustor, which acts as a fuel-rich, hot-gas generator for the supersonic combustor. The major portion of the air bypasses the gas generator and is ducted supersonically through an air conduit to the supersonic combustor, where it mixes and burns with the exhaust of the gas generator. The final shocks shown in the supersonic duct (depicted as two sets of intersecting oblique waves) result from the combustion-induced pressure disturbances generated by the supersonic combustion process. The region is commonly referred to as the combustor/inlet interaction region.

COMBUSTOR/INLET INTERACTIONS

Experimental Program

Data from connected-pipe tests of Dual Combustion Ramjet combustors h ve shown the existence of a precombustion pressure rise beginning in the annular supersonic flow upstream of the gas generator base and extending into the supersonic combustor (Ref. 1). This precombustion pressure rise is being simulated in a simplified test setup using overexpanded cold air in order to

develop a data base over a wide range of test conditions and geometries. Fig. 2 on p. 7 is a schematic and photograph of the DCR Combustor/Inlet Interaction (CII) test hardware. The annular isolator duct that conducts supersonic air to the supersonic combustor surrounds the sonic or supersonic exhaust flow from the gas generator simulator. Test variables include the annulus Mach number (1.75, 2.4 and 3.0) and Reynolds number, the gas generator exit Mach number (1.0 to 2.5), the airflow split between the supersonic annulus and gas generator (1:1 to 6:1), and the length of constant area duct downstream of the exit of the gas generator. The primary instrumentation includes wall and instream pressure measurements.

The data from this experimental program will be used to:

(1) yield a data correlating equation that will define the location and extent of the precombustion compression field in the annular isolator duct that conducts compressed air from the engine inlet to the supersonic combustor as a function of the appropriate variables;

(2) describe the boundary layer growth, statistics of the turbulence and average flowfield property radial profiles in the annular isolator duct; and

(3) measure pitot pressure radial profiles in the supersonic combustor section at various axial stations downstream of the gas generator base.

Data correlations from the CII test program will be used in conjunction with the DCR combustor test data to design inlet air ducts which will prevent the precombustion pressure disturbance from disrupting the external air inlet flowfield.

Results

Various procedures have been evaluated to calculate the instream flow properties in a supersonic annular flowfield from measured instream pitot

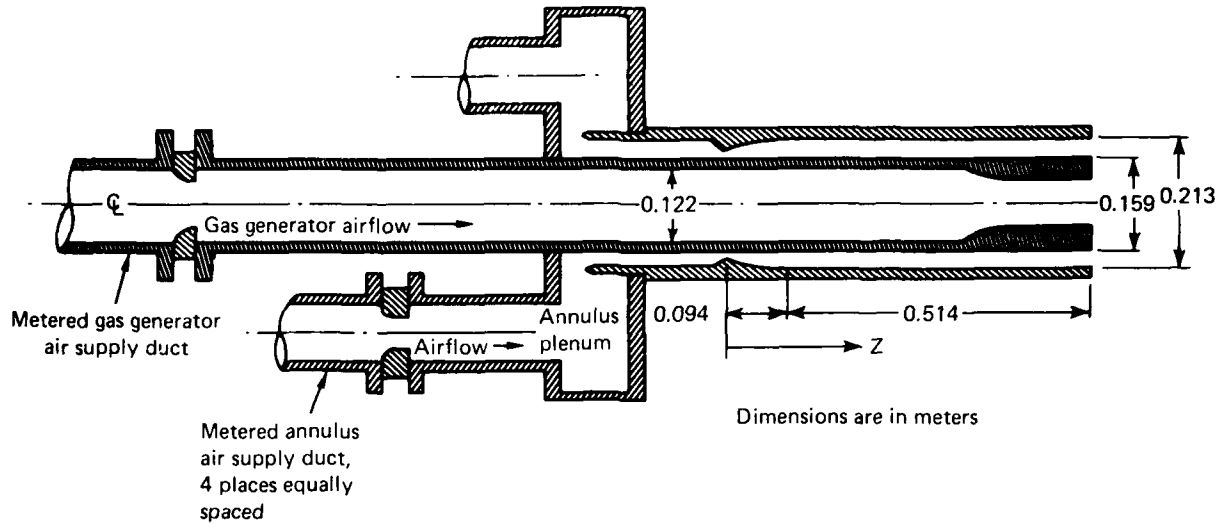

(a) Schematic of hardware

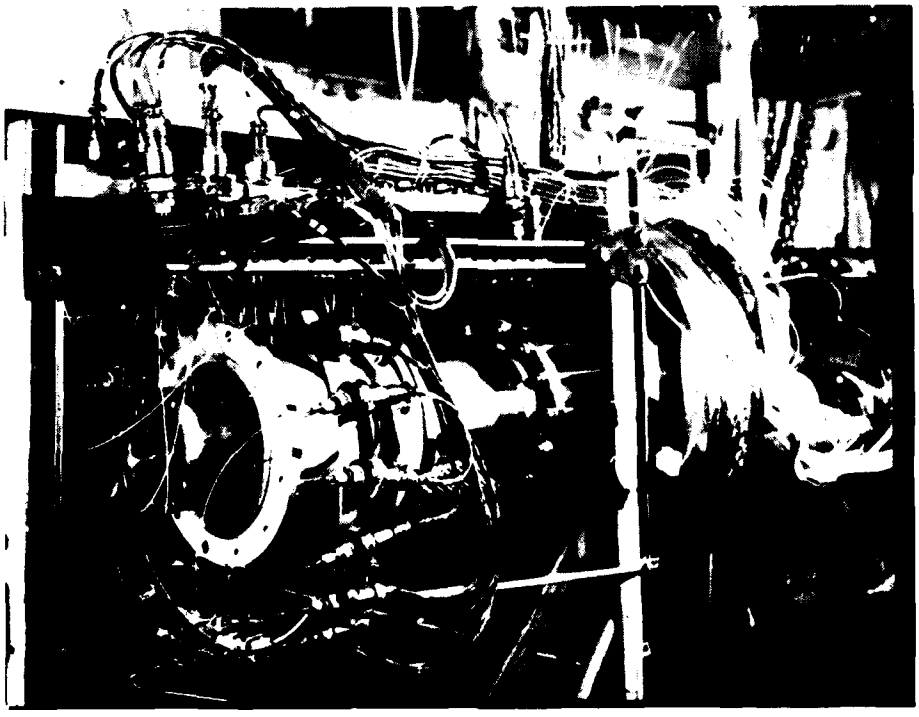

(b) Photograph of hardware

Fig. 2 DCR shock-wave interaction test setup.

pressures, wall pressures and plenum conditions. Each procedure achieves analytical closure on all flowfield property variations by deriving the values for a second instream flowfield property as a function of the radial (r) and axial (z) position based on various theoretical premises. One procedure assumes a constant static pressure across the annular duct equal to the average of the five measured wall pressures at that axial station. Another procedure assumes a constant static pressure which conserves mass at that station. A third variation assumes a static pressure profile at each axial position that is quadratic with respect to the radius r, conserves mass and matches the measured static pressures at the wall. All of these procedures were found to be unsatisfactory (Refs. 2, 3). One reason for this was that some of the computed instream total pressures (p_t) at various radii were higher than the measured plenum total pressure, thereby violating entropy constraints. Two additional unsatisfactory results of these initial assumptions were: (1) the calculated displacement thicknesses and turbulence intensities were unrealistic; and (2) the correlation of the fluctuating components of density and velocity (avg. of $\tilde{\rho}\,\tilde{u}$) close to the walls was greater than zero. These difficulties were exacerbated by the high sensitivity of Mach number and total pressure to small variations in the assumed instream static pressure profile.

A new procedure has been developed that (1) conserves mass; (2) matches the measured wall pressure; (3) ensures that the stagnation entropy never decreases in the flow direction; and (4) correctly models the effects of viscosity both in the center of the duct and next to the walls. This procedure assumes a symmetric radial total pressure profile, $p_t(r, z)$, that is constant and equal to the plenum total pressure (p_{t_o}) over a central inviscid core at the center of the duct, and is quadratic with respect to distance from the midpoint between the annular walls for the two wall regions (see Fig. 3 on p. 9). The quadratic curve fit allows three constraints to be imposed: (1) zero slope at the junction of the quadratic with the central inviscid core segment, (2) matching of the centerline total pressure (p_{t_o}), and (3) matching of the wall pressure. The position of the junction point is determined iteratively to conserve mass. This new integral analysis overcomes all of the deficiencies of the previous methods while retaining their desirable properties (conserving mass and matching the measured wall static pressures).

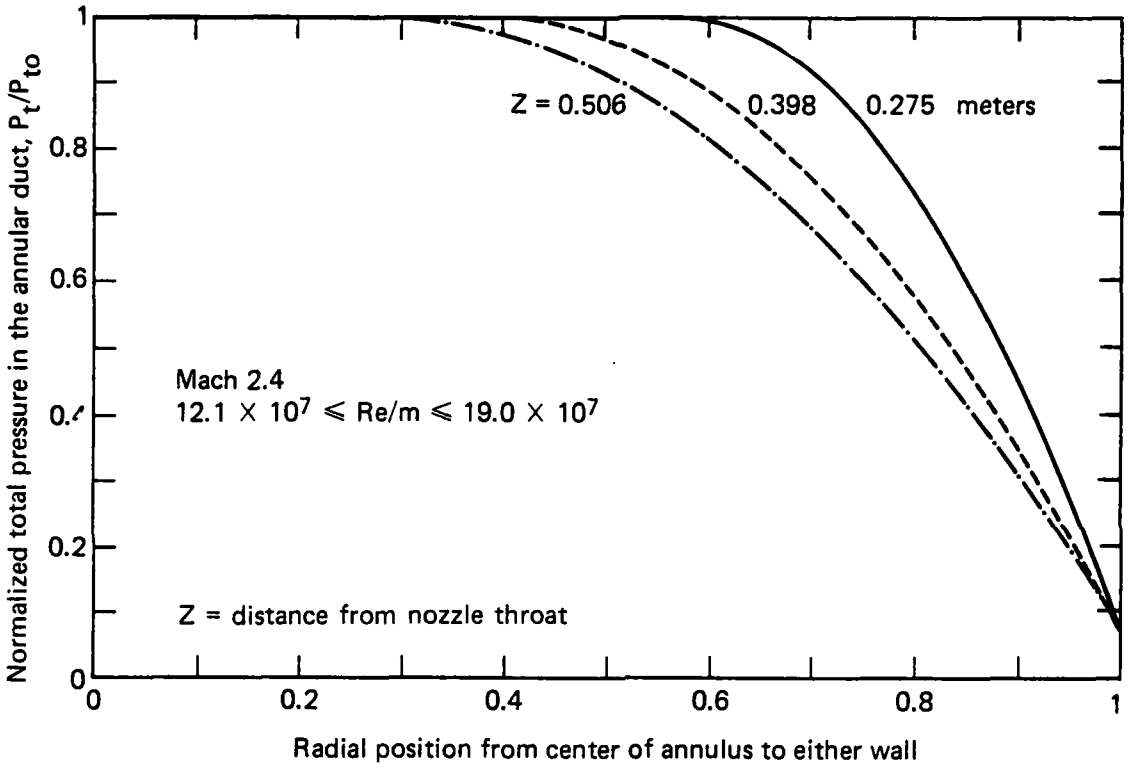

Fig. 3 Assumed total pressure radial profiles in the CII annular duct normalized with respect to the plenum total pressure calculated to match the plenum and wall pressures and to conserve mass.

Fig. 3 on page 9 shows $p_t(r, z)$ for the three axial positions (z) in the annular isolator duct for which pitot pressure p_t' measurements were made. The variable z is the distance from the annular nozzle throat to the designated axial position. Fig. 3 on page 9 shows graphically the growth of the viscous wall region and the decay of the inviscid core as the flow progresses downstream.

The determination of the boundary layer thickness, δ, displacement thickness, δ^*, momentum thickness, Θ, and kinetic energy thickness, δ_{KE}, affords a quantitative measurement of the importance of viscosity in the DCR combustor/inlet isolator duct. These data are important in the determination of the required geometric area divergence for the isolator duct in the DCR engine and in the development of a data-correlating equation that specifies the location of the precombustion compression field in the isolator duct as a function of various parameters that may include δ^* and/or Θ (Ref. 4). The equations defined in Ref. 5 for these thicknesses are listed in Table 1 on p. 11. They are for compressible, axisymmetric flow around or within a body with transverse radius R. For the annulus inner wall boundary layer thicknesses, the flowfield is external and R is positive, whereas the opposite applies for the annulus outer wall.

Fig. 4 on p. 12 shows the calculated boundary layer thickness plotted against z. There was no change in these boundary layer results when the Reynolds number, Re, was varied from 12.1 to 19.0 x 10^7/m. At the end of the 0.513 m long constant area annular duct (z = 0.607 m), the fractions of the total cross-sectional area (0.016 m^2) occupied by the various boundary layer thicknesses are 74% for δ, 13% for δ^*, 7.6% for δ_{KE} and 4.2% for Θ.

As shown in Figs. 5-8 on p. 13 and 14, this boundary layer growth affects the mean flowfield property variations with respect to z. At the center of the duct, for z increasing from 0.275 to 0.506 m downstream of the nozzle throat, the Mach number, M, falls from 2.42 to 2.33, the velocity, u, falls from 565 to 555 m/sec and the mass flux, ρu (ρ = density), rises from 1220 to 1308 kg/m^2-sec. Note also the effect of the boundary layer growth on the average values of these properties in the boundary layer. As expected, both the Mach number and velocity are retarded at a fixed distance from either

Table 1
Defining equations for integral thicknesses.

Displacement thickness δ^*:

$$\delta^* + \frac{\delta^{*2}}{2R} = \int_0^\delta \left(\rho - \frac{\rho u}{\rho_\delta u_\delta}\right)\left(1 + \frac{y}{R}\right) dy$$

Momentum defect thickness θ:

$$\theta + \frac{\theta^2}{2R} = \int_0^\delta \frac{\rho u}{\rho_\delta u_\delta}\left(1 - \frac{u}{u_\delta}\right)\left(1 + \frac{y}{R}\right) dy$$

Kinetic energy defect thickness δ_{KE}:

$$\delta_{KE} + \frac{\delta_{KE}^2}{2R} = \int_0^\delta \frac{\rho u}{\rho_\delta u_\delta}\left(1 - \frac{u^2}{u_\delta^2}\right)\left(1 + \frac{y}{R}\right) dy$$

R = transverse body radius whose sign is positive for external and negative for internal flows
u = velocity
ρ = density
δ = boundary layer edge
y = distance from wall

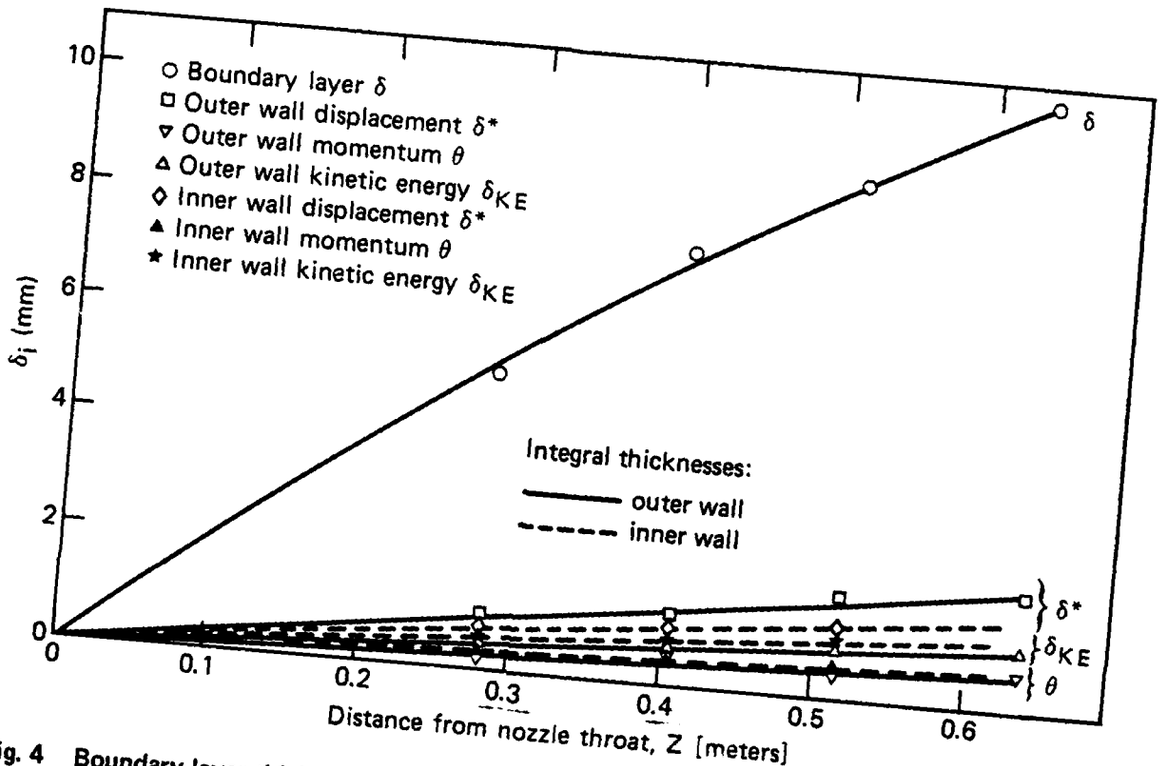

Fig. 4 **Boundary layer thicknesses along the annular walls in the combustor/inlet interaction tests isolator duct for Mach 2.4 and 12.1X10*7 ⩽ RE/m ⩽ 19.0X10*7.**

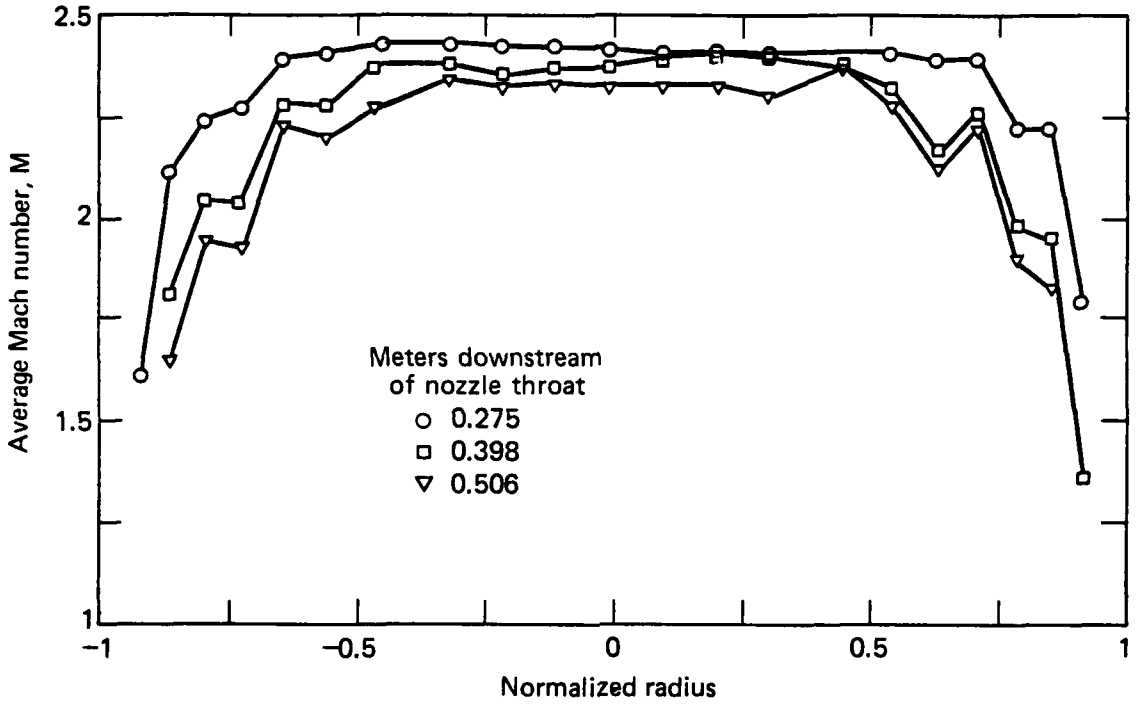

Fig. 5 Average Mach number vs. radial position in the CII Mach 2.4 annular flowfield.

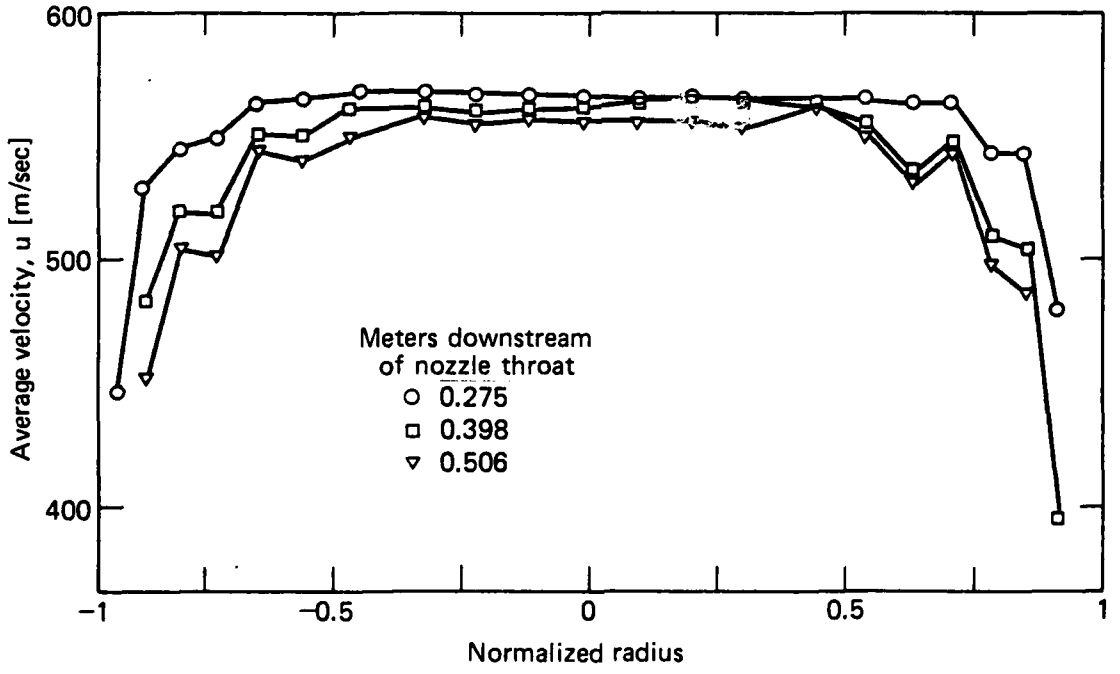

Fig. 6 Average velocity vs. radial position in the CII Mach 2.4 annular flowfield.

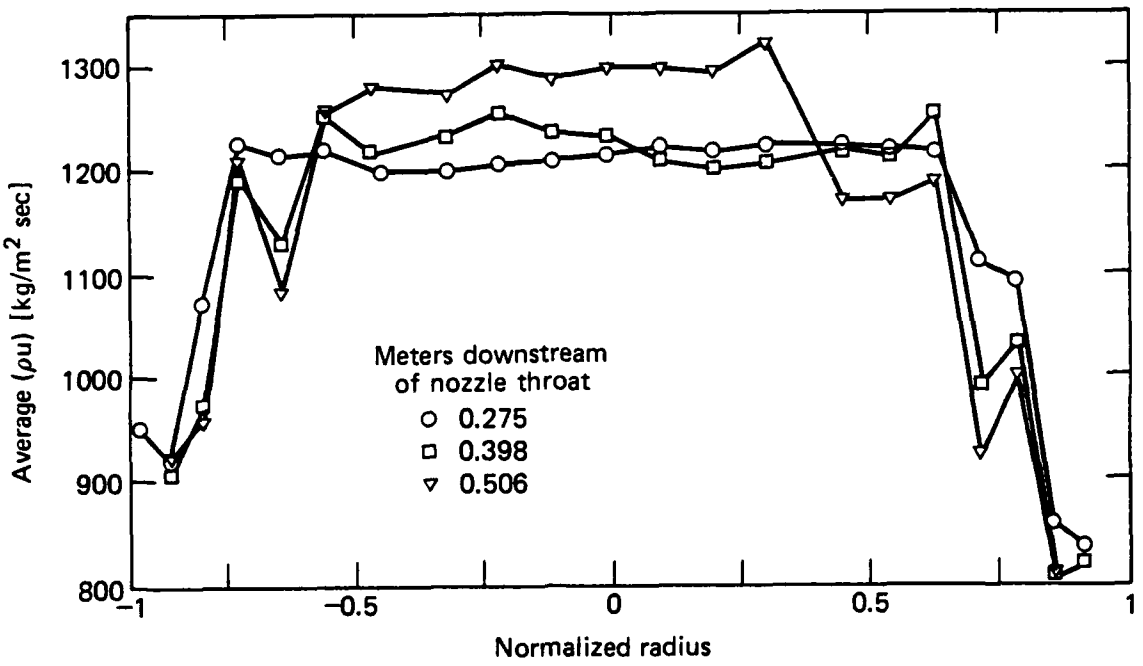

Fig. 7 Average mass flux vs. radial position in the CII Mach 2.4 annular flowfield.

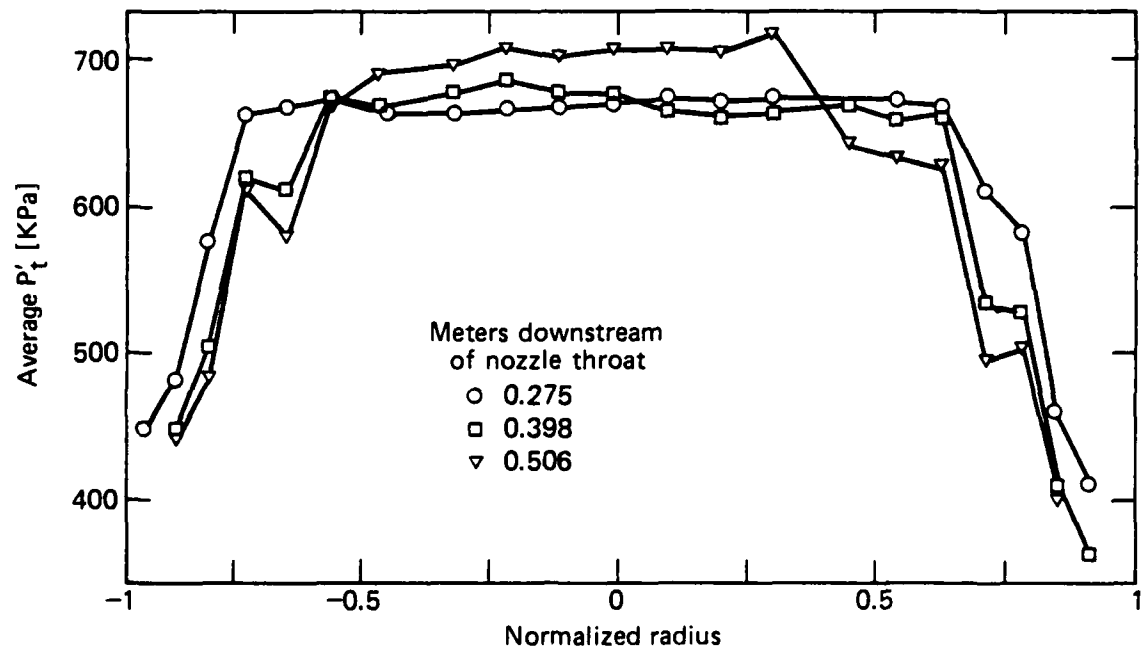

Fig. 8 Average Pitot pressure vs. radial position in the CII Mach 2.4 annular flowfield.

wall as the boundary layer grows in the downstream direction. The non-smooth pattern for ρu in the boundary layer is also evident in the average pitot pressure data (p_t', Fig. 8 on p. 14), which is the experimentally measured data upon which all property calculations depend. While the p_t' curve for $z = 0.275$ m shows a continuous rise in p_t' with distance from either wall, the departure from this expected behavior is moderate for $z = 0.398$ m and more severe at $z = 0.506$ m in <u>both</u> wall regions. Thus, the consistency of this pattern with respect to variations in z and for either the inner or outer wall supports the validity of the measured results.

The results for M and u in Figs. 5 and 6 on p. 13 are invariant with respect to the above Reynolds number range. The ρu and p_t' plots in Fig. 7 and 8 on p. 14 are for $Re/m = 12.1 \times 10^7$ and a plenum total pressure $p_t = 1241$ kPa. The curves for these quantities at $Re/m = 19 \times 10^7$ are similar in every respect except absolute magnitude.

In order to quantify the magnitude of the fluctuating component of various flowfield properties in the CII annular isolator duct, the root mean squares (rms) of the time series for the fluctuating component of the pitot pressure p_t', velocity u, density ρ and mass flux ρu have been computed. Note that the time average of the fluctuating component of any property time series is zero. These computed results have been normalized with respect to the average value of the specified property at the radial position in the annular duct for which the velocity is a maximum for that axial station. Figs. 9-12 on p. 16-17 show these data, respectively, plotted against the normalized radial position where the data were measured for three axial positions in the CII isolator duct, $z = 0.275$, 0.398 and 0.506 m downstream of the annular nozzle throat. The last station, $z = 0.506$, is 0.1 m upstream of the gas generator base. In these figures, a fluctuating component of a flowfield property is designated by a superscript tilda and an average value by a superscript bar.

These results show that the intensity of the turbulence is highest in the boundary layer and increases as the boundary layer thickens. In the CII isolator duct, viscosity and its various ramifications, such as significant boundary layer growth, boundary layer influence on the mean flow and

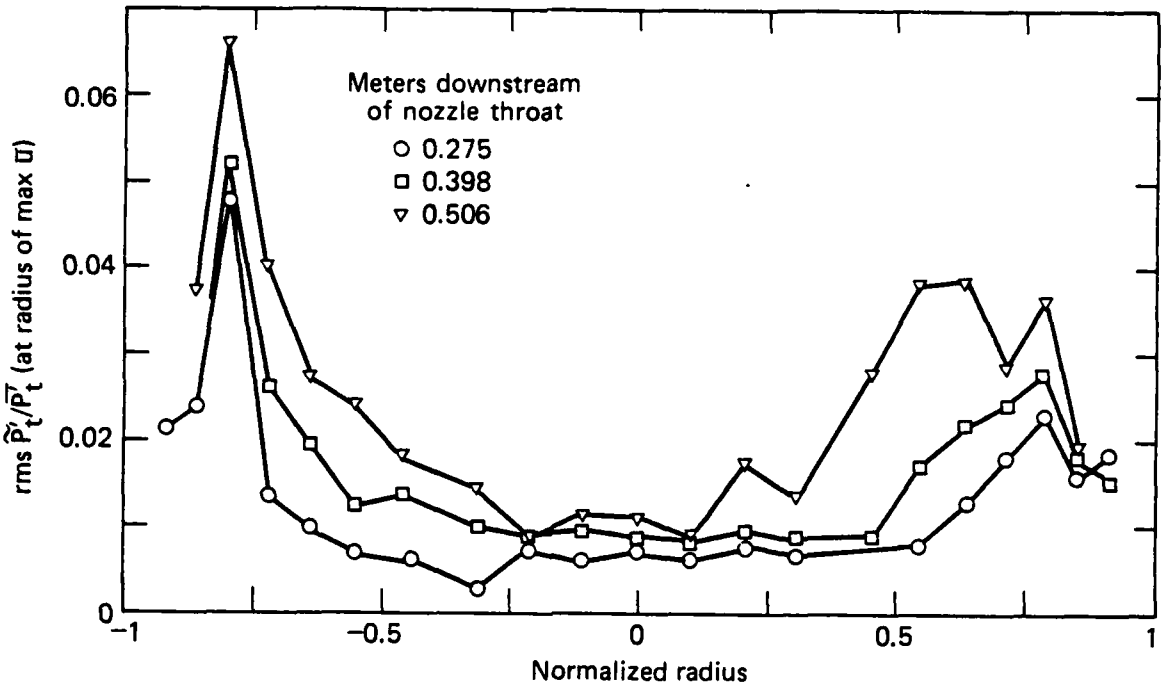

Fig. 9 Pitot pressure fluctuations in the Mach 2.4 ducted flowfield.

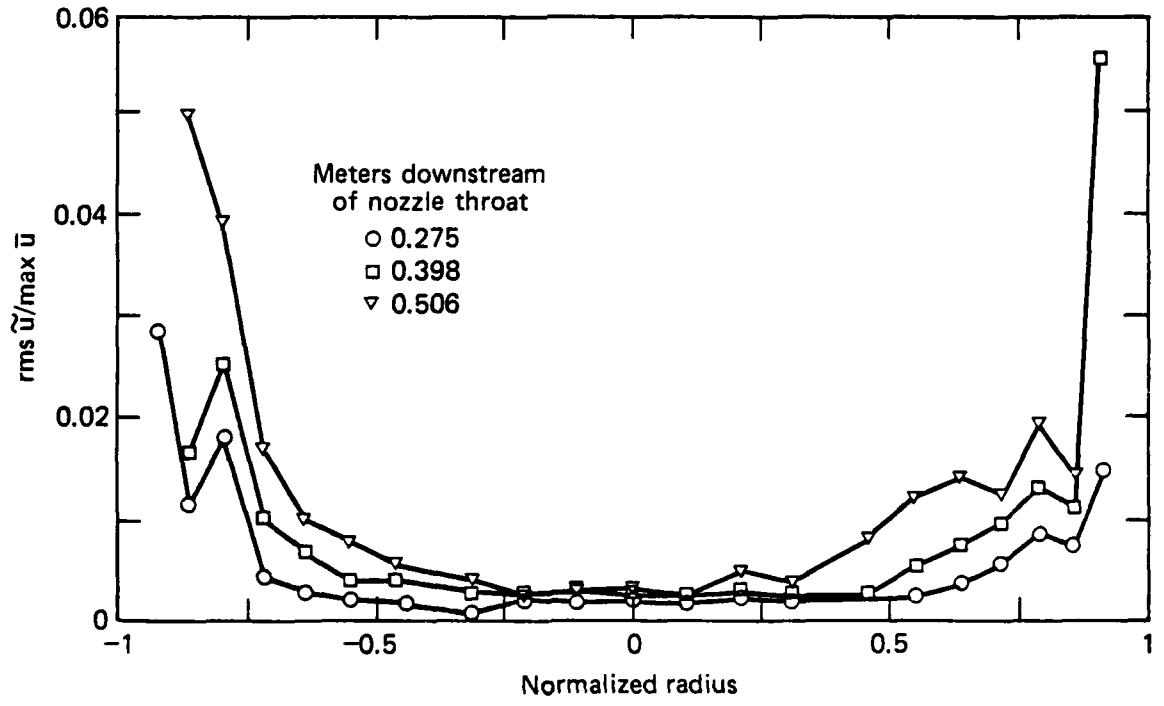

Fig. 10 Velocity fluctuations in the Mach 2.4 ducted flowfield.

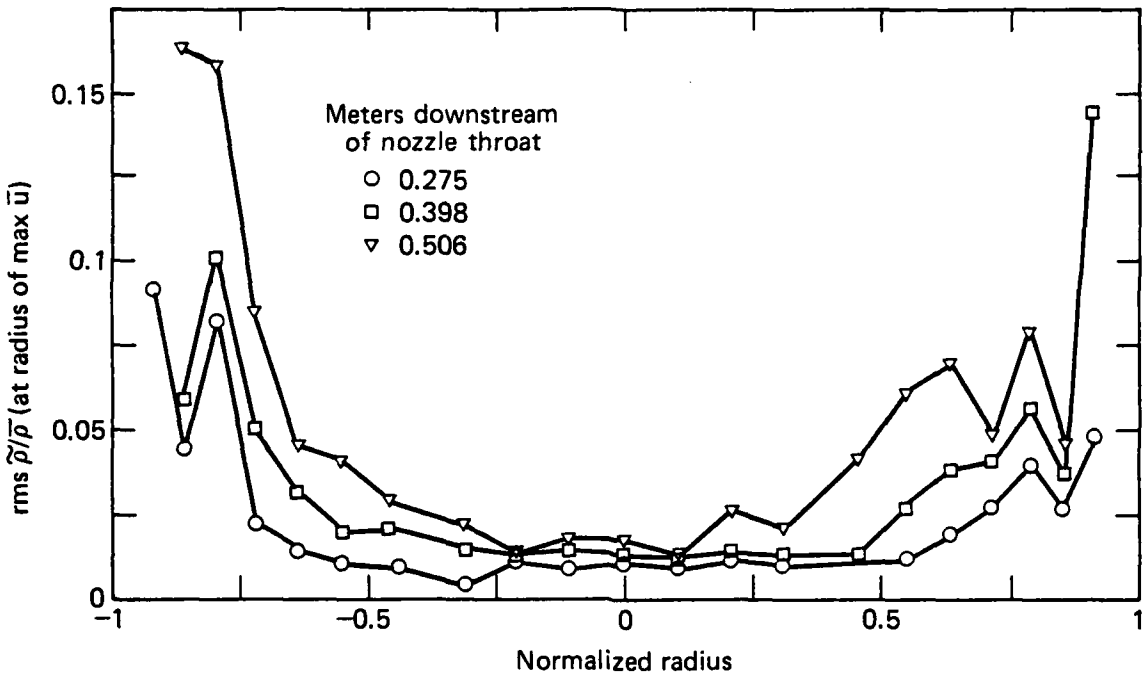

Fig. 11 Density fluctuations in the Mach 2.4 ducted flowfield.

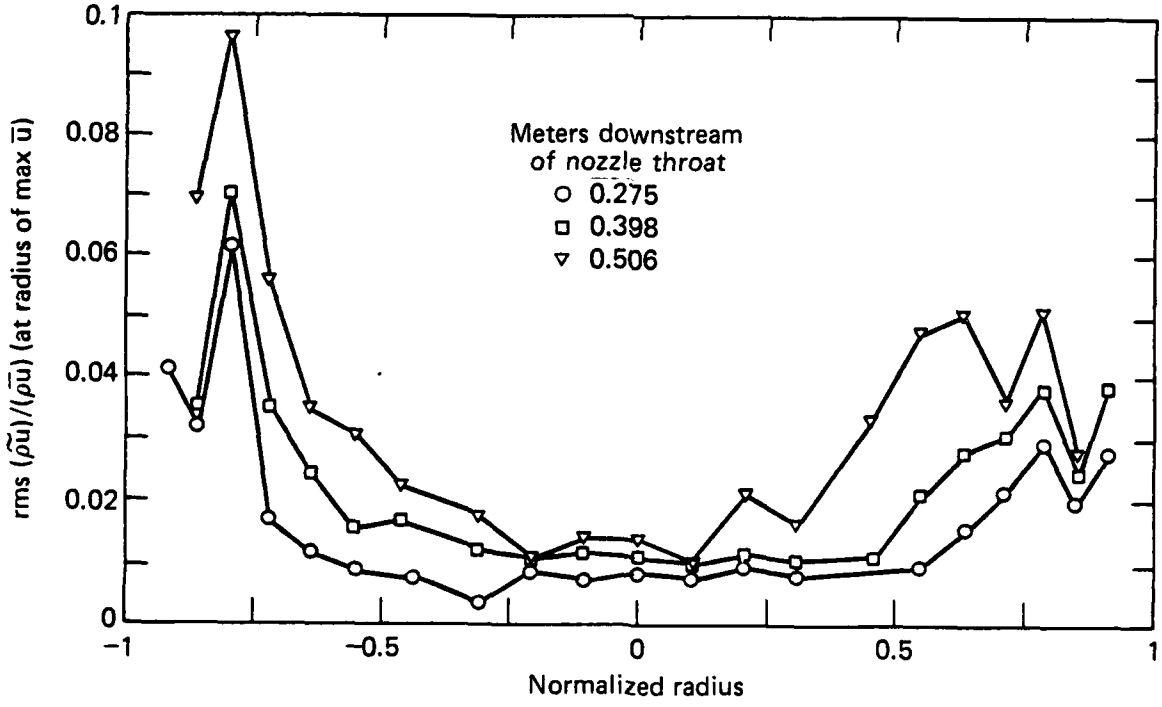

Fig. 12 Mass flux fluctuations in the Mach 2.4 ducted flowfield.

boundary layer turbulence, dominate the flow dynamics. These results are based upon the calculated instream total pressures in Fig. 3 on p. 9.

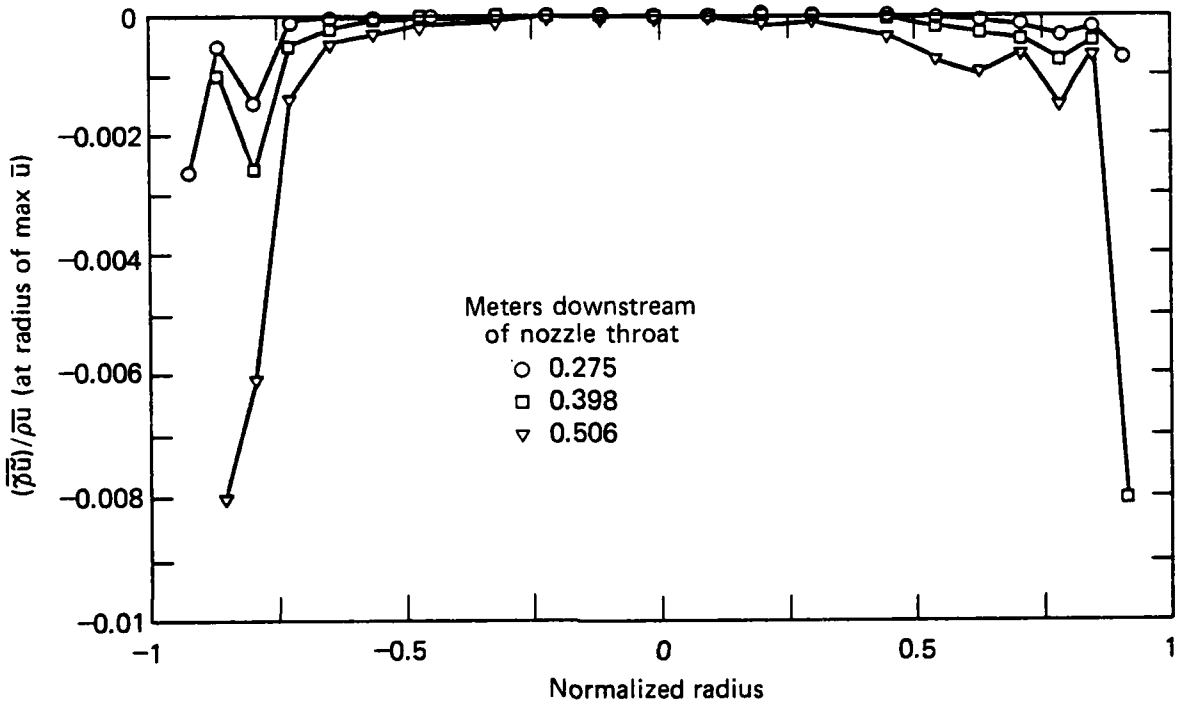

Fig. 13 Correlation of velocity and density fluctuating components in the Mach 2.4 ducted flowfield.

Fig. 13 shows that the statistical correlation of ρ and u in the duct is zero outside of the boundary layer and negative inside the boundary layer. This is an expected result, typical of turbulent boundary layers, and while primarily of theoretical interest, does offer an important confirmation of the validity of the computational procedure.

The investigation of the simulated precombustion compression field in the overexpanded annular flowfield is the primary purpose of this experimental investigation. The calculation of δ, δ^*, Θ and δ_{KE} throughout the annular duct from measured data has been completed primarily so that one or more of these thicknesses can be incorporated into the correlating equation that will be derived to predict the precombustion compression field location. Ref. 4 shows that Θ was an important parameter in an analogous

correlation for the pure scramjet geometry. The location and length of the simulated precombustion compression field is a function of t e following test variables: (1) the degree of overexpansion relative to ambient exhaust conditions; (2) the mass flow ratio ($\dot{w}_a/\dot{w}_g$) between the outer annular and inner gas generator flows; (3) the gas generator exhaust nozzle Mach number and contour; (4) the length of duct that extends downstream from the end of the annulus; and (5) the annular nozzle Mach number. These items are being systematically varied over the entire experimental range of interest. Figs. 14-16 on p. 20-22 show various measured wall pressure distributions that simulate the precombustion compression field. A pressure rise ratio greater than the normal shock pressure rise ratio for the actual nozzle exit Mach number (2.4) has been obtained (Fig. 14 on p. 20) for a case where $\dot{w}_a/\dot{w}_g = 0.506$. This actual mass flow split corresponds to an effective mass flow split of 1.04 when the effect of the maximum temperature difference between the two streams in the operating engine is included. Fig. 16 on p. 22 shows the isolated effect of varying $\dot{w}_a/\dot{w}_g$. For high $\dot{w}_g$, the gas generator flow expands supersonically, lowers the base pressure and has the aspirating effect of translating downstream the position of the compression field in the annulus. This allows a greater degree of overexpansion and, consequently, a higher overall pressure rise ratio.

Discussion

The value of the boundary layer integral thicknesses δ^*, Θ, and δ_{KE} are very sensitive to the value of the boundary layer thickness δ, which is usually defined to be the distance from the wall at which the local average velocity is equal to 0.99 times its "freestream" value. This sensitivity enters the equations in Table 1 on p. 11 through the ρ_δ and u_δ quantities in the integral equations and through the δ limit of integration. For an internal flowfield with a static pressure gradient normal to the wall (the CII flowfield), there is not, in general, a definitive value for δ because there is no definitive "freestream" velocity (Ref. 5, p. 19). Because the integral thicknesses are very sensitive to the value of δ, it is recommended in Ref. 5 for supersonic flows that δ be defined as the thickness of the region next to the wall in which the local total pressure increases to 99% of its original (plenum) value. This definition removes the ambiguity

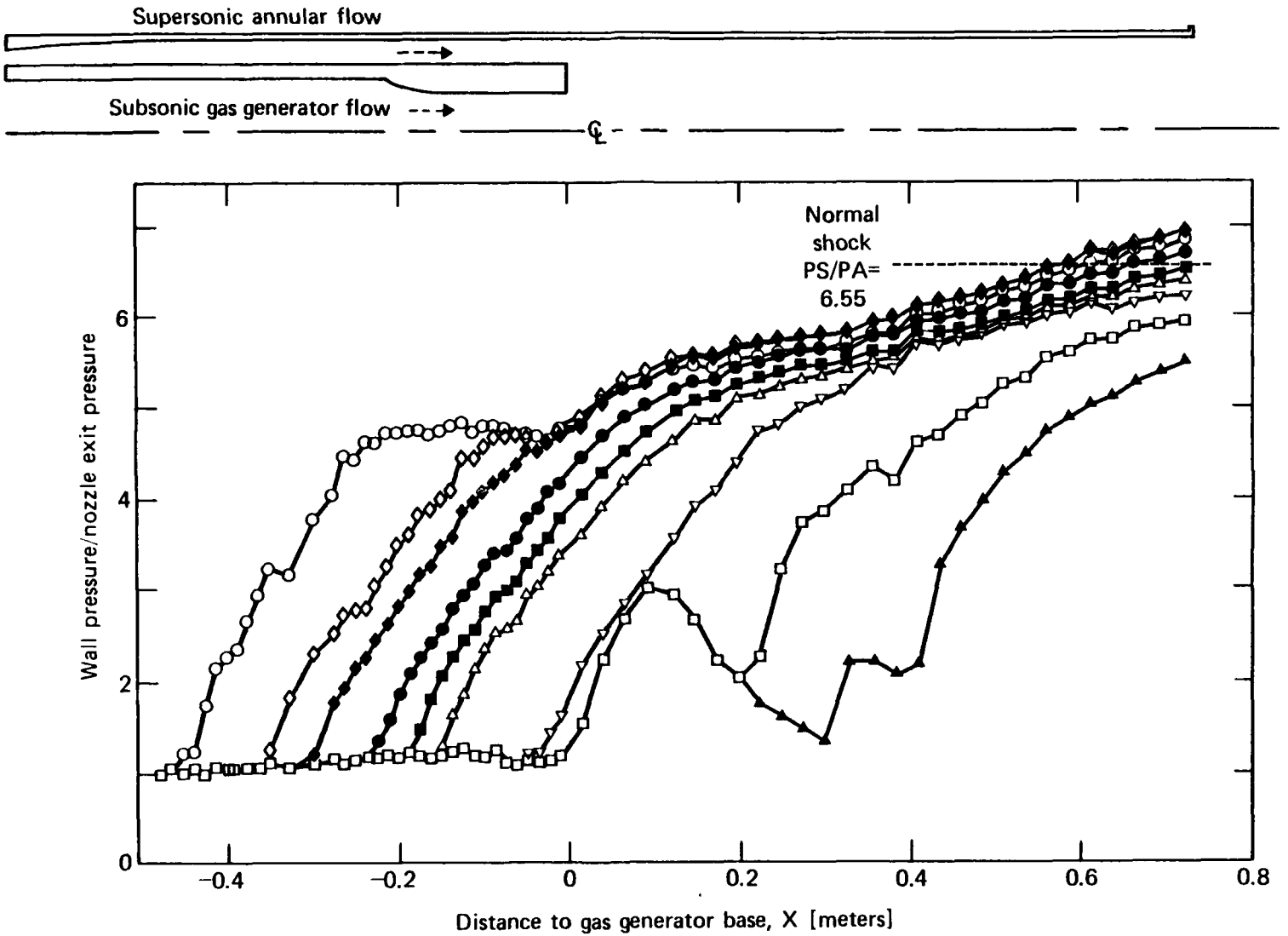

Fig. 14 **Wall pressure distributions in the CII hardware with a long cylindrical duct section downstream of the annulus.**

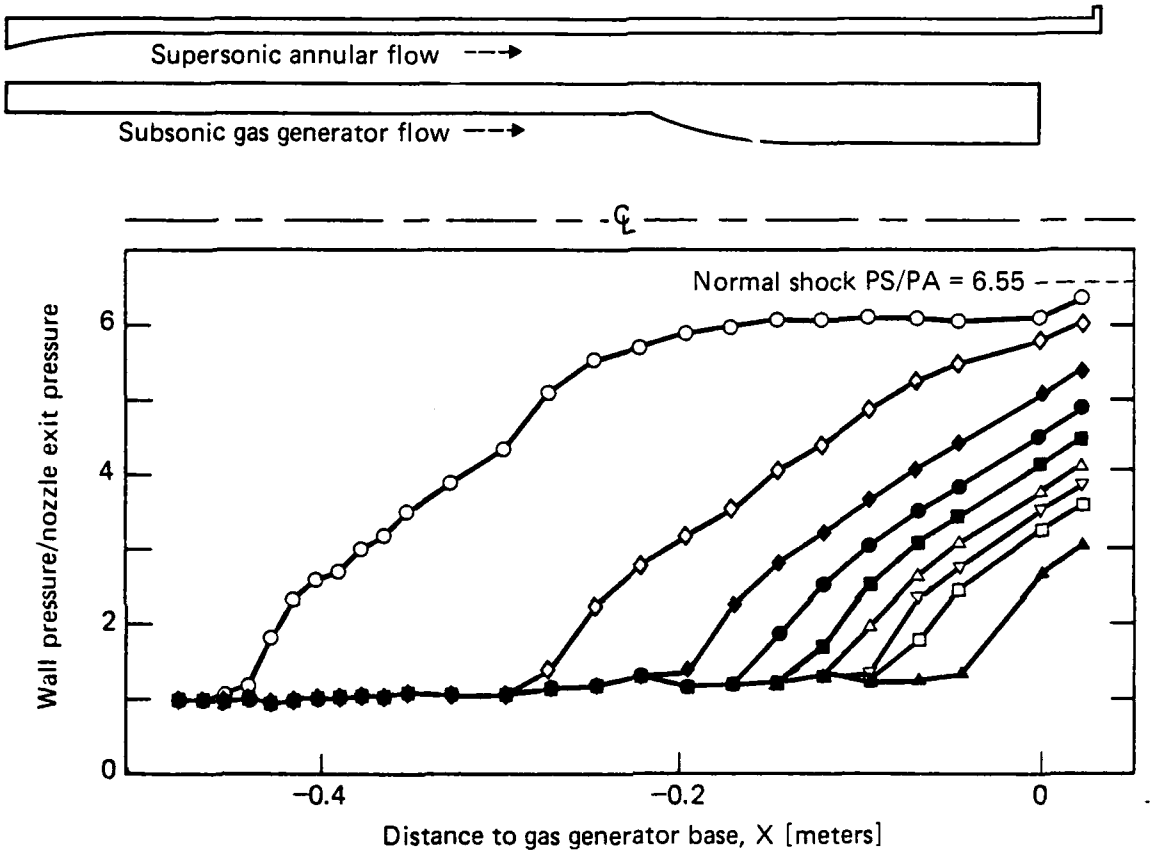

Fig. 15 **Wall pressure distributions in the CII annular duct.**

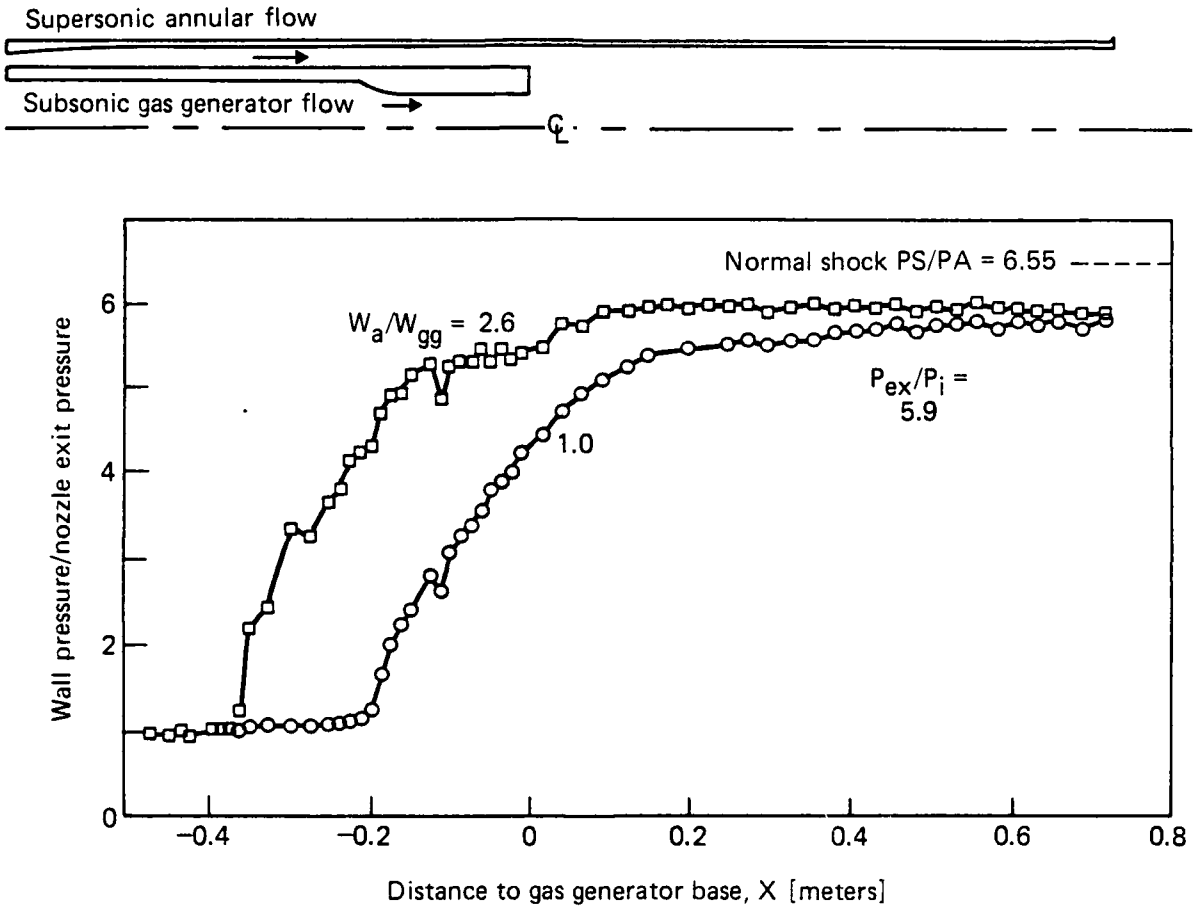

Fig. 16 Effect of mass flow ratio variation on precombustion compression field wall pressure distribution.

that would arise if the velocity ratio were used and provides a common basis of comparison. It is also philosophically consistent with the total pressure quadratic curve fit analytical closure procedure that is used here to calculate instream properties. On the basis of these arguments and on the numerical results of calculating the integral thicknesses based on different criteria for the selection of δ, this total pressure-based δ definition has been used consistently in the integral thickness calculations presented in this report.

The CII experimental results are compared in Tables 2-4 on p. 24-25 to compressible turbulent boundary layer data obtained by other investigators. In these tables, y is the distance from the wall. When used as a subscript, δ indicates the value of a property at the boundary layer edge. All of the turbulent fluctuation data in the surveyed literature (Refs. 6-9) came from velocity measurements using hot wire anemometers. The comparable CII data came from measuring the pitot pressure with both a high response Kulite brand miniature pressure transducer and with Alinco brand pressure transducers. Although a direct comparison of the flow property statistics determined from a hot wire and from these pressure transducers for the same flowfield has not been made, the CII data in Tables 2-4 on p. 24-25 compares favorably with the other data, particularly in the supersonic Mach number range for the velocity data. Table 5 on p. 26 summarizes some of the boundary layer data at the 3 axial locations in the CII annular duct where pitot pressure radial profiles were measured. The Reynolds number Re_Θ range was 40-68 x 10^{-3}.

The Kulite brand miniature pressure transducer frequency response is flat to 20 kHz, whereas the cutoff frequency of the Alinco is only 75 Hz. Both are silicone-diaphragm, strain-gauge transducers. The Kulite transducer has no internal volume (the diaphragm is an external surface of the transducer); it was mounted in the flow at the tip of a pitot probe. The Alinco transducers have 0.25 in^3 internal volume between the entrance port and the pressure-sensitive diaphragm; they were connected to the pitot probes with about 1 ft of 0.065 in. inner diameter Nylon tubing, which added an additional 0.04 in^3 or 16% to the internal volume. The Kulite was positioned in the approximate center of the inner boundary layer at a normalized radial

Table 2
Comparison of turbulent velocity fluctuation u′ results with other compressible turbulent boundary layer data.

	M_δ	rms u′ (y)/ Avg u (y)		Max* rms u′ (y)/ Avg u (δ)
	(Z, cm)	Max* (y/δ)	at y = δ (δ, mm)	(y/δ)
Stockbridge	2.38	0.036	0.003	0.029
	(27.5)	(0.217)	(5.3)	(0.217)
	2.37	0.079	0.003	0.055
	(39.8)	(0.156)	(7.3)	(0.156)
	2.33	0.062	0.005	0.050
	(50.6)	(0.217)	(8.9)	(0.217)
Kistler	1.72	0.065	0.005	0.051
(Ref. 6)		(0.159)	(17.8)	(0.159)
	3.56	0.080	0.006	0.060
		(0.135)	(26.7)	(0.135)
	4.67	0.068	0.004	0.045
		(0.071)	(29.21)	(0.130)
Waltrup	2.38	0.073	0.009	
(Ref. 7)		(0.38)	(9.32)	
	1.95	0.052	0.006	
		(0.234)	(9.60)	
Owen	7.2	0.081	0.011	0.052
(Ref. 8)		(0.04)	(33.0)	(0.04)
Laderman	9.4	0.096	0.0006	
(Ref. 9)		(0.013)	(141)	

*Max refers only to the maximum of the available tabular data.

Table 3
Comparison of turbulent density fluctuation ρ' results with other compressible turbulent boundary layer data.

	M_δ	rms ρ' (y)/ Avg ρ (y)		Max* rms ρ' (y)/ Avg ρ (δ)
	(Z, cm)	Max* (y/δ)	at y = δ (δ, mm)	(y/δ)
Stockbridge	2.38	0.090	0.015	0.088
	(27.5)	(0.217)	(5.3)	(0.217)
	2.37	0.147	0.018	0.140
	(39.8)	(0.156)	(7.3)	(0.156)
	2.33	0.173	0.023	0.146
	(50.6)	(0.370)	(8.9)	(0.217)
Owen	7.2	0.10	0.067	0.062
		(0.43)	(33)	(0.56)
Laderman	9.4	0.137	0.026	
		(0.543)	(141)	

*Max refers only to the maximum of the available tabular data.

Table 4
Comparison of $(\dot{w}/A)'$ results with other compressible turbulent boundary layer data.

	M_δ	rms $(\dot{w}/A)'$ (y)/ Avg $(\dot{w}/A)$ (y)		Max* rms $(\dot{w}/A)'$ (y)/ Avg $(\dot{w}/A)$ (δ)
	(Z, cm)	Max* (y/δ)	at y = δ (δ, mm)	(y/δ)
Stockbridge	2.38	0.068	0.012	0.060
	(27.5)	(0.541)	(5.3)	(0.541)
	2.37	0.086	0.014	0.069
	(39.8)	(0.389)	(7.3)	(0.389)
	2.33	0.116	0.019	0.088
	(50.6)	(0.320)	(8.9)	(0.320)
Owen	7.2	0.15	0.065	0.025
		(0.04)	(33)	(0.04)

*Max refers only to the maximum of the available tabular data.

Table 5
CII boundary layer data at three axial positions in the annular isolator duct.

	Distance from nozzle throat, z [m]		
	0.275	0.398	0.506
δ [mm]	5.3	7.3	8.9
δ^* [mm]	1.0	1.1	1.8
θ [mm]	0.3	0.5	0.5
δ_{KE} [mm]	0.6	0.9	1.0
M_δ	2.38	2.37	2.33
$Re_\theta \times 10^{-3}$	40.4	61.8	68.0
T_δ [°K]	139	139	139
rms $u'(\delta)$ [m/sec]	1.58	1.92	2.62
rms $\rho'(\delta)$ [kg/m^3]	0.032	0.032	0.048
rms $(\rho u)'$ (δ) [kg/m^2 sec]	15.29	17.62	23.67
$\overline{u}$ (δ) [m/sec]	560.5	559.6	554.1
$\overline{\rho}$ (δ) [kg/m^3]	2.194	2.178	2.306

Note: All values for integral boundary layer thicknesses are the largest for both walls.

position, R, of -0.79 and accounts for the spike in the property fluctuation plots at that radius. It is significant that the maximum values for rms u' and rms ρ' were measured with Alinco transducers at radii closer to both walls than R = -0.79 because it shows that the limited bandwidth of the Alinco transducers did not change the trend of the correlation of turbulence intensity with proximity to either annular wall.

The Kistler data (Ref. 6) in Table 2 on p. 24 were obtained at a single station on the flat wall opposite flexible two-dimensional (2D) nozzle plates. The Reynolds number Re_Θ range was 26 to 35 x 10^{-3}. The static pressure was constant through the boundary layer, and the test section walls were adiabatic.

The Waltrup and Schetz data (Ref. 7) in Table 2 on p. 24 is for a 2D turbulent boundary layer along a test section wall that is subjected to an adverse pressure gradient by the insertion of a ramp into a 2D nozzle. The Reynolds number Re_Θ range was 20 to 40 x 10^{-3} and the walls were adiabatic.

The Owen data (Ref. 8) in Tables 2, 3, and 4 on p. 24-25 came from the Mach 7.2 external flowfield about an axisymmetric body. The test boundary layer was formed on a 10^o semiapex angle cone-ogive-cylinder 3.3 m long and 0.203 m in diameter. The wall temperature was only half the recovery temperature and Re_Θ = 13 x 10^{-3}.

The Laderman data (Ref. 9) in Tables 2 and 3 on p. 24-25 came from a boundary layer that was formed on the upper wall of a contoured 2D flexible nozzle and test section. There was severe heat transfer to the wall; the wall temperature was 0.4 times the recovery temperature. The test surface was polished to a micro-in. finish and the wall was actively cooled. The Reynolds number Re_Θ was 40 x 10^{-3}, and the Mach number was 9.4.

COMPONENT AND ENGINE CYCLE MODELING

Rather than develop a single model describing the complete DCR supersonic combustor and exit nozzle flow processes, one which would be

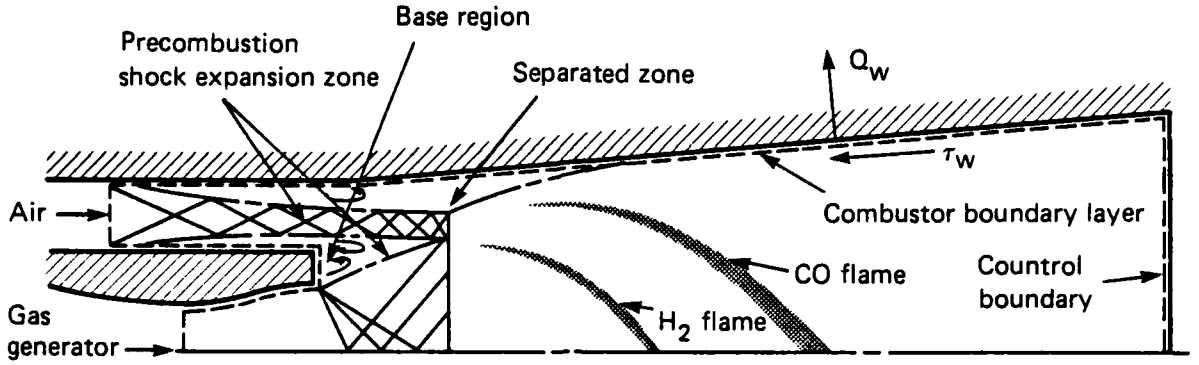

Fig. 17 Theoretical model for combustion analysis.

extremely complex and prohibitively expensive to use, an alternative, "building block" approach has been adopted. This approach permits each distinct region (Fig. 17) downstream of the combustor entrance, viz., the base flow, central core flow and wall boundary layer, to be described separately and then matched to each other. Since each region is amenable to certain simplifying physical assumptions not necessarily applicable in another region, this approach permits a simpler, yet physically realistic description of each region compared to an all-encompassing analysis, and a complete solution is orders of magnitude less expensive to obtain.

Fig. 17 illustrates the region of interest in these analyses. The shocks shown in the supersonic duct result from the combustion-induced pressure disturbances generated by the mixing and heat release processes. The region is commonly referred to as the combustor/inlet interaction region. With no heat release, the shock structure is not present and expansion waves are possible depending on the geometry and flow conditions in the inner jet. With heat release, the pressure rise associated with this shock system can vary from low values equivalent to those corresponding to oblique waves up to the value corresponding to a normal shock in the incoming air. Thus, at low Mach number and high heat release rates, the flow in the main combustor is subsonic, which is the mode of operation in the conventional "scramjet" or "dual-mode" engine (Ref. 10).

A modular approach to the analysis of this complex flowfield has been adopted. Fig. 17 on p. 28 also shows the regions of flow that are handled in these modules. The mixing and burning of the central portion of the flow is the main module and will ultimately use input from modules that treat the shock structure in the incoming outer flow and from a module that handles a detailed treatment of the "base region" of the injector. A separate module is used to calculate the wall boundary layer and then is coupled to the main flow solution. This approach is made necessary by the substantial difference in grid resolution required in these two parts of the flow. A much finer grid is required in the boundary layer than in the mixing and burning zone, so that wall properties can be accurately predicted.

One of the important complicating features of the flow in the combustor is the recirculation region in the base of the thick "lip" of the gas generator exhaust (Fig. 17 on p. 28). The flow in this region interacts with the hot exhaust jet and the inlet air to determine the pressure and the other flow variables at the beginning of the mixing and burning region in the main combustor. The accurate prediction of the subsequent flow in the combustor is clearly dependent upon the determination of good "initial conditions" as a result of an analysis of this base flow.

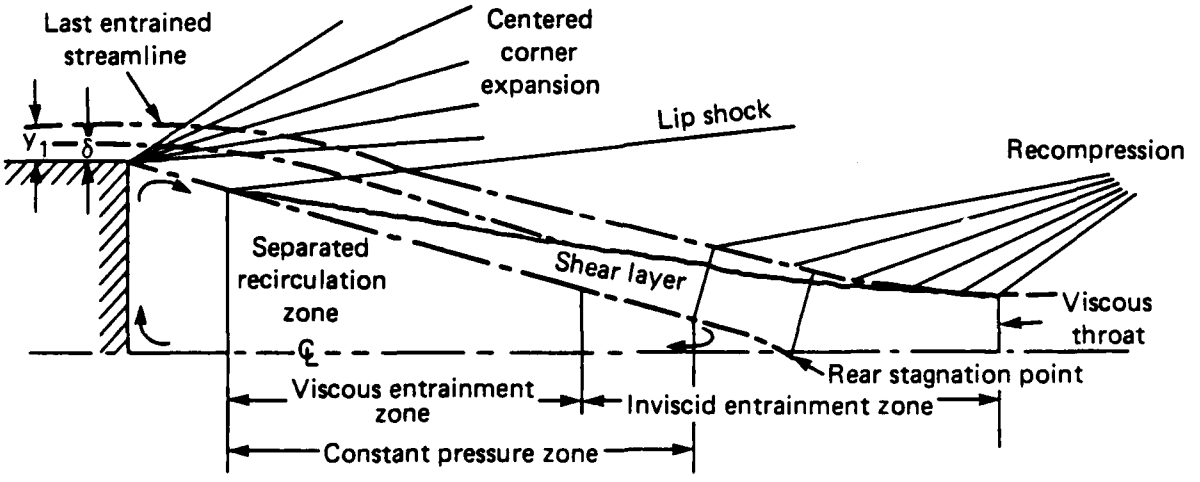

Fig. 18 Schematic illustration of base flow entrainment model.

The flowfield for a simple, planner base is shown schematically in Fig. 18 on p. 29. The analysis of this complex flow has been compartmentalized. The flow in the upstream boundary layer and some of the inviscid flow above the boundary layer is taken inviscidly through the corner expansion and the lip shock. None but the most complicated existing analyses include the lip shock. The subsequent downstream flow outside of the viscous base region is also treated as inviscid. The viscous treatment of the flow in the base begins at the viscous throat and proceeds upstream. The flow from the viscous throat to the rear stagnation point is analyzed using generalized versions of the methods in Refs. 11-14. The flow in the region above the dividing streamline through the rear stagnation point and upstream from the rear stagnation point to the downstream end of the constant pressure region is treated using integrated equations of motion but with the pressure gradient taken as predicted for a centered wave pattern. A unique composite solution for the whole is selected by requiring continuity of the mass flow in the shear layer from the downstream and upstream proceeding portions of the analysis.

Some comparisons of predictions and experiments for the planar base flow are given in Figs. 19 to 21 on p. 31-33. Figs. 19 and 21 show predicted and experimental centerline pressure distributions at two upstream Mach numbers in the range of interest. Clearly, the base pressure and the major features of the flow are well predicted. Fig. 20 on p. 32 shows that the important effects of the size of the upstream boundary layer are adequately accounted for.

The main mixing and burning calculations can currently be made with either a greatly extended version of the code presented in Ref. 15 or the Los Alamos VNAP-II code developed by M. C. Cline. The former is based on the boundary layer (parabolic) formulation of the equations of motion and the latter is a full axisymmetric solution of the Navier-Stokes equations, which permits the important effects of pressure feedback and radial pressure gradients to be included. The extensions, in each case, include the integrated, turbulent kinetic energy (TKE) method for calculating the eddy viscosity (following Ref. 16), the double-flamesheet model of Ref. 17, the chemical equilibrium calculation procedure of Ref. 18, and the integral, confined flow

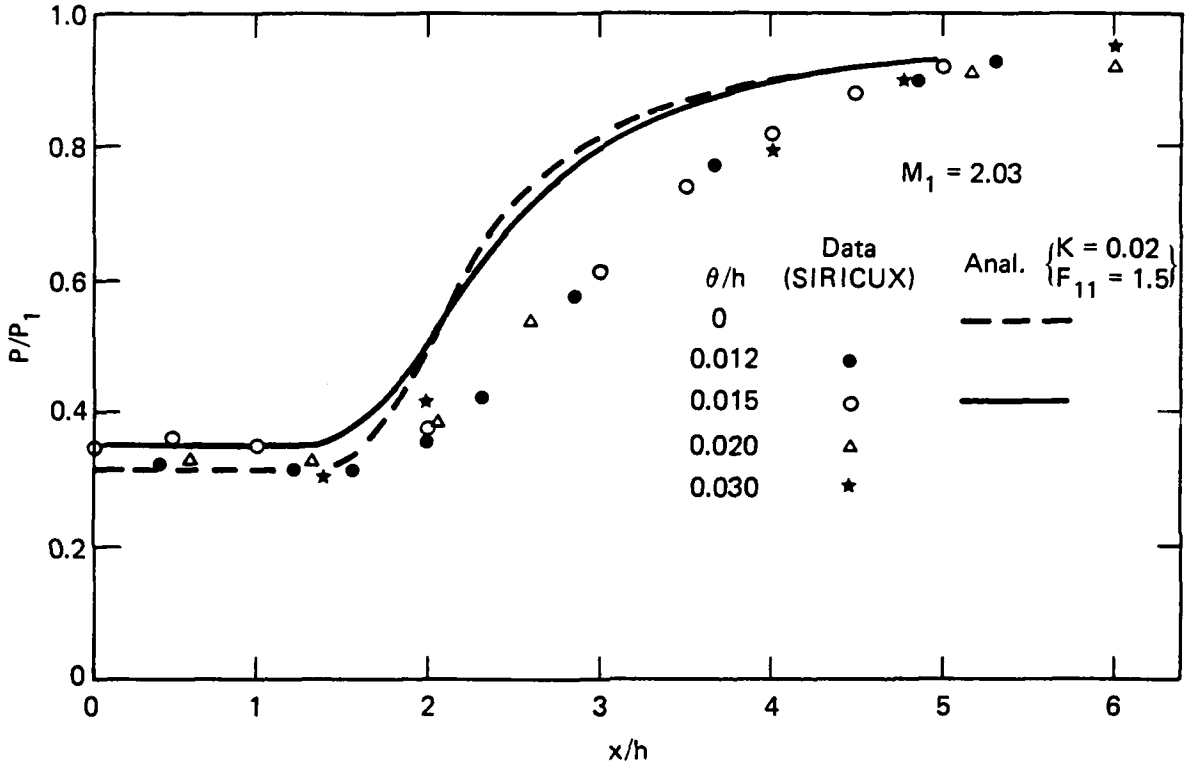

Fig. 19 Prediction and experiment for pressure distribution behind a base at $M_1 = 2.03$.

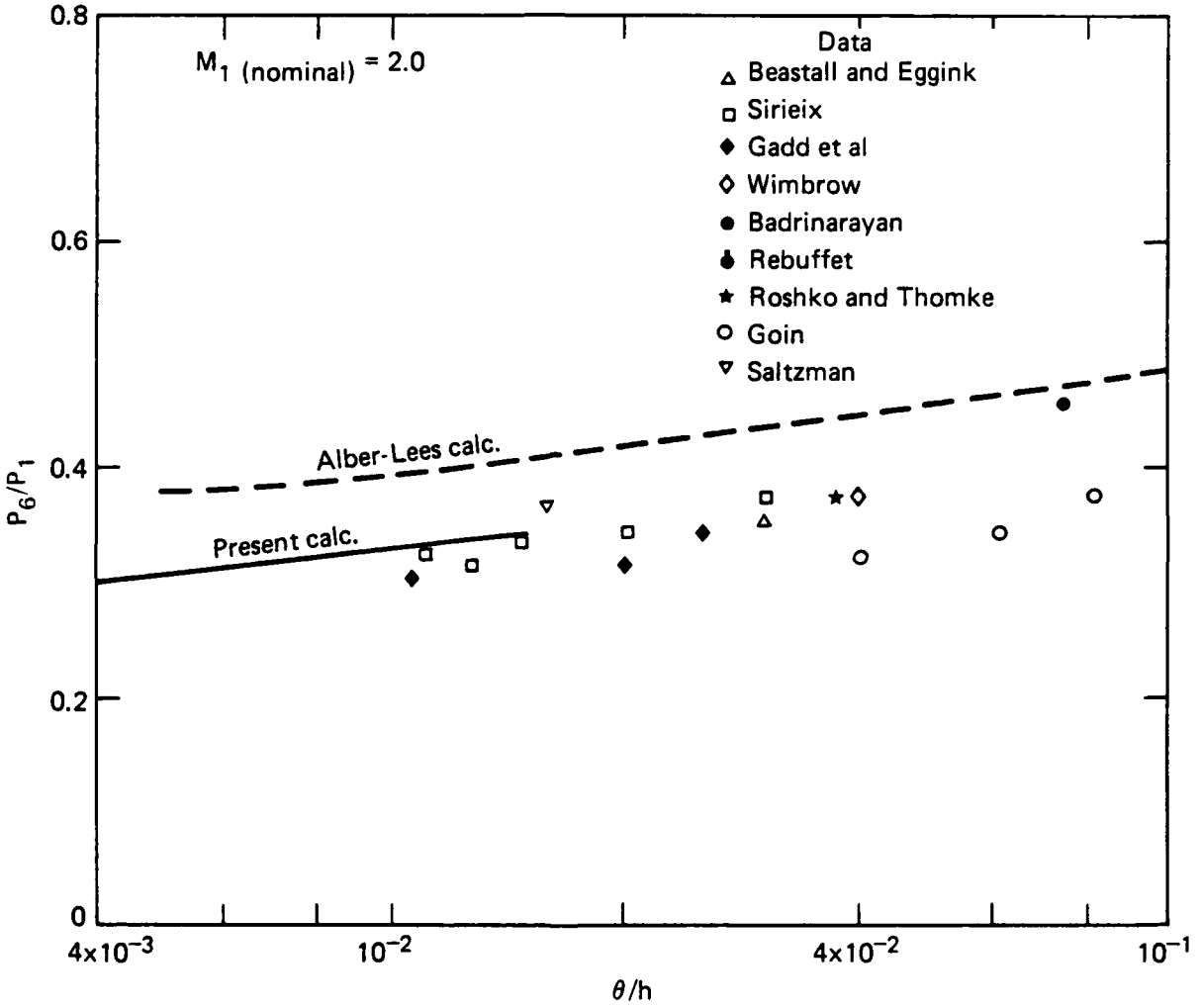

Fig. 20 Effect of upstream boundary layer momentum thickness on base pressure.

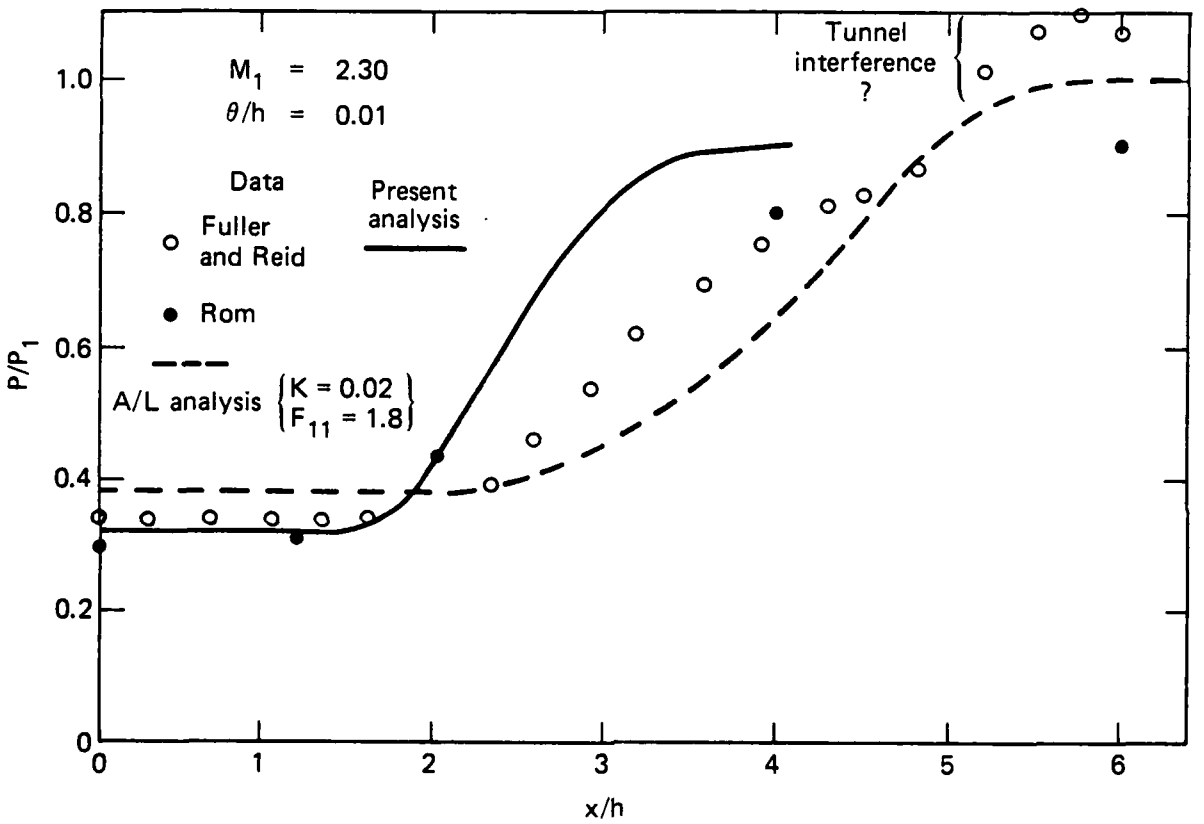

Fig. 21 Predictions and experiments for pressure distribution behind a base at M_1 = 2.30.

with heat release treatment of Refs. 10 and 19. For the parabolic formulation, the first extension was to accommodate confined mixing in a duct with a central fuel jet rather than jet mixing in an infinite stream as had been done in Ref. 20. This was accomplished by holding the stream function ψ along the outer boundary fixed at its initial value ψ_{MAX} in order to maintain a constant total mass flow in the duct. Velocity "slip" was allowed along the duct wall. Two options are incorporated: in option 1, $p(z)$ is specified and the cross-sectional area $A(z)$ is computed; in option 2, the inverse is done. The second extension incorporated a more advanced turbulent transport model in both of these options. An integrated equation for turbulent kinetic energy was used to predict the variation of eddy viscosity along the duct following the method in Ref. 16. The third and largest extension incorporated equilibrium chemical reactions into the mixing zone.

The C-H-O-N chemical system is written to include the following species: O_2, N_2, H_2, CO, CO_2, OH, O, H, N, and NO. Because of the high static pressures and temperatures and the need to reduce the problem to manageable proportions, local diffusion-controlled chemical equilibrium was assumed. The computer code given in Ref. 18 was modified extensively to reduce the cost per calculation for an enthalpy-pressure entry by an order of magnitude, to about one cent per point. Still further simplifications were necessary to bring the computation cost to an acceptable level. For example, about 25 radial points with 1000 axial stations are required to obtain acceptably accurate solutions in a 0.1-m radius, 2-m-long duct. At one cent per point, the cost of the equilibrium calculations is about \$250-\$500, compared to less than \$50 for the remainder of the entire mixing calculations.

To decrease the number of required equilibrium calculations, the double-flamesheet model of Ref. 17 was adapted to the present problem. Simply stated, the model comprises an inner H_2 flame and an outer CO flame with only the O_2, H_2, N_2, H_2O, CO, and CO_2 species assumed to be present. As long as the temperature remains below about 2500°K, the model provides a good approximation to the exact equilibrium state. Therefore, a composite model was adopted. At each axial station, a complete calculation is made using the double-flamesheet model. The temperature profile is searched for points having a predicted temperature greater than 2500°K. For those points, a

complete equilibrium calculation is made before moving to the next axial station. The resulting cost reduction factor has been about three to five.

The fourth extension was necessary because the hot combustion products from the main mixing and burning region are in the shear layer at the outer edge of the wall boundary layer, and they significantly affect wall heat transfer and skin friction. Furthermore, the turbulence produced in that shear layer influences the wall boundary layer, just as high free-stream turbulence affects an aerodynamic boundary layer. Therefore, a prediction of the turbulence level in the shear layer was needed. The TKE model was changed from one based on an average value of TKE across the mixing zone (Ref. 16) to one that includes the solution of a partial differential equation for the detailed distribution of the TKE model. The modeling follows the Prandtl Energy Method (Ref. 21).

One important point remained. Since the parabolic mixing and burning code is based on the boundary layer form of the equations of motion, no upstream influence is possible. On the other hand, it is well known that heat released in a supersonic flowfield inside a duct can affect the initial conditions (Ref. 10). This critical behavior was included by using the integral analysis of Refs. 10 and 19 to set the initial conditions and $p(z)$ along the duct.

For the boundary layer calculations, adoption or adaptation of existing codes (or parts of codes) was sought. There are a number of elaborate computer codes for boundary layer flows for turbulent, high-speed flow conditions (e.g., Refs. 22 and 23). A comprehensive review of codes for numerical calculation of reacting, laminar boundary layer may be found in Ref. 23, but none is suitable for a scramjet combustor because the chemistry generally is limited to air (no burned fuel species) and because provisions to account for the rapidly varying boundary-layer "edge" conditions under turbulent conditions have not been included. The necessary extension involved not only the C-H-O-N chemistry but also significant complications in terms of the viscosity, Prandlt number and Lewis number of the resulting mixture. There are also important new questions with regard to the modeling of turbulent transport processes in these types of flows.

The modified code uses the basic finite difference methods of Ref. 22 for the numerical solution of the equations of motion and the chemistry and physical properties procedures of Ref. 25. The required modifications of the code of Ref. 22 included: a) an added routine for the solution of the diffusion equations, b) additions to the routine for the solution of the energy equation to account for energy transport as a result of diffusion and for streamwise variation of the edge conditions on total enthalpy, c) revision and/or replacement of routines that relate enthalpy to temperature and species concentrations and those that calculate the equation of state, d) establishment of proper calling sequences for the new physical property subroutine, and numerous other minor modifictions. To reduce the computing cost per call, the code of Ref. 25 was substantially modified to operate as a subroutine, and the calculation procedures were streamlined and simplified to the C-H-O-N system. The routine was also modified so that the transport property routines could be called without going through the equilibrium composition calculations, if desired.

The boundary layer flows of interest differ from those for simpler aerodynamic cases in two important ways. First, the products of combustion are diffusing in from the outer edge. This changes the distribution of density and physical properties across the whole layer. Second, the rapidly varying boundary layer edge conditions result in profiles of atypical shape in the outer part of the layer. Hence, it is inappropriate to apply turbulent transport models that have been developed and tested only for conventional boundary layer flows. A model more fundamental than the algebraic eddy viscosity or mixing model of Ref. 21 was sought. The new model is based on the variation of the kinetic energy turbulent fluctuations,

$$k \equiv \frac{\tilde{u}^2 + \tilde{v}^2 + \tilde{w}^2}{2}, \qquad (1)$$

in the flow. Prandtl (Ref. 21) suggested the form of one such approach. A turbulent viscosity, μ_T, is related directly to k with a length scale, ℓ, as

$$\mu_T = \rho \sqrt{k\ell} \qquad (2)$$

The variation of ℓ is specified algebrically, but a separate conservation equation that includes k must now be solved along with the other equations of motion. Importantly, the equation for k involves terms for the production and dissipation of turbulence that depend upon the profile shape. Thus, turbulent transport is made sensitive to any new processes that influence profile shape (see, e.g., Refs. 26 and 27). This model has been implemented in the modified wall boundary layer code.

The accurate prediction of nozzle flows for ramjets and scramjets is important for efficient design and accurate system performance analysis. The problem is made complex by the presence of strongly nonuniform nozzle entrance profiles typical of scramjets, which have no sonic throat at the end of the combustor. Thus, turbulent mixing and perhaps chemistry can be expected to be underway during the expansion process. The rapid expansion common in nozzles of practical configuration implies substantial radial pressure gradients also. Taken all together, these requirements imply the necessity of utilizing a formulation based on the full Navier-Stokes equations for a compressible, multi-component, turbulent flow with finite rate chemistry.

This work was begun with the VNAP2 code developed by M.C. Cline at Los Alamos for compressible, single-component, turbulent flow without chemistry. Diffusion equations for 10 species were added, as were additional terms in the energy equation for energy transfer due to mass transfer. Finite rate chemistry for a system with N-C-O-N atoms in various molecular combinations was also included.

The extension of the VNAP2 code to consider cases with varying composition involves a considerable effort. For example, the changes to the energy equation involve not only the additional terms for energy transfer but also additional terms for varying molecular weight. These arise because the energy equation is used with the equation of state to develop an equation that is used to calculate the pressure.

The VNAP2 code is based on MacCormack's explicit method, and it thus has step size restrictions from the flowfield calculation. Adding provisions for finite rate chemistry introduces step size restrictions from the

chemistry. If the time scales involved are of greatly different orders of magnitude, computational instability problems can result. However, from a practical point of view, these potential problems do not occur, since the use of this code can be restricted to cases for which the two time scales are of a similar order of magnitude. If the two time scales are of a different order of magnitude, we have the following alternatives. If the chemical times are very short compared to flow times, we assume local equilibrium. If the chemical times are very long compared to flow times, we use finite rate chemistry calculations by themselves.

The Navier-Stokes formulation of the jet mixing/combustion code is the preferred choice at this time because it includes all of the features of the parabolic formulation but permits pressure feedback and radial pressure gradients, an important feature when computing exit nozzle flowfields. Currently, refinements being added to the analyses include a more detailed description of the base-like flow region downstream of the lip of the gas generator based on modifications of the analyses developed in Refs. 16-20 and 28, as well as a description of the combustor/inlet interaction region once it is completed. These will provide more detailed initial conditions for both the boundary layer and core flow models. In addition, a "two-fluid" set of equations is planned for incorporation in both the core flow and boundary layer codes to assess the effects of liquid and/or solid particles in a flow of this type. Extension of the flamesheet/equilibrium model and inclusion of physical property routines (to avoid the binary diffusion approximation currently used) in the boundary layer code are also planned.

Results

The analysis of the coaxial mixing and combustion region is used to insure an adequate length of combustor for complete burning and to predict the level of non-uniformity of the combustor exit flow entering the nozzle. The primary goals of the wall boundary layer calculations are predictions of the local heat transfer and skin friction. The heat transfer must be known to design engine cooling systems and structure, and the skin friction in the combustor must be known to calculate overall system performance (e.g., gross thrust). The present wall boundary layer analysis includes the important

effects of entrainment of combustion products from the coaxial flame into the boundary layer.

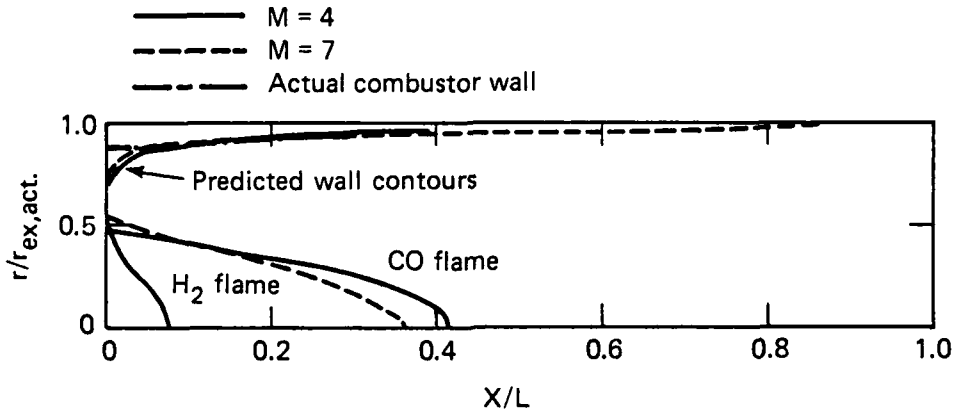

Fig. 22 Predicted combustor wall and flame sheet contours for M_0 = 4 and 7 flight with ER = 0.5.

The shape and length of the two flames illustrated in Fig. 17 on p. 28 are predicted at typical Mach 4 and 7 flight conditions as shown in Fig. 22 on p. 39. The longest flame is for CO combustion; it is about 1 meter long, whereas the H_2 flame is about 0.2 meters long. Fig. 23 on p. 40 presents the corresponding predicted central core temperature and species profile at Mach 7 with a fuel-air equivalence ratio, ER, of 0.5.

The edge conditions for the boundary layer calculations were obtained from the coaxial jet mixing and burning code. Fig. 24 on p. 41 shows the streamwise variation of the skin friction coefficient and wall heat flux for Mach 7 flight with ER = 0.5. Here, calculated values of wall skin friction and heat transfer show that both increase with increasing combustor heat release, a result observed in past experiments on supersonic combustion ramjet engine combustors (Ref. 29). The sensitivity of the local heat transfer to the local character of the pressure distribution is also illustrated by the steep rise of the local heat transfer in the air duct ahead of the combustor where a strong shock structure is located. Fig. 25 on p. 42 presents the boundary layer CO_2 concentration, temperature and velocity

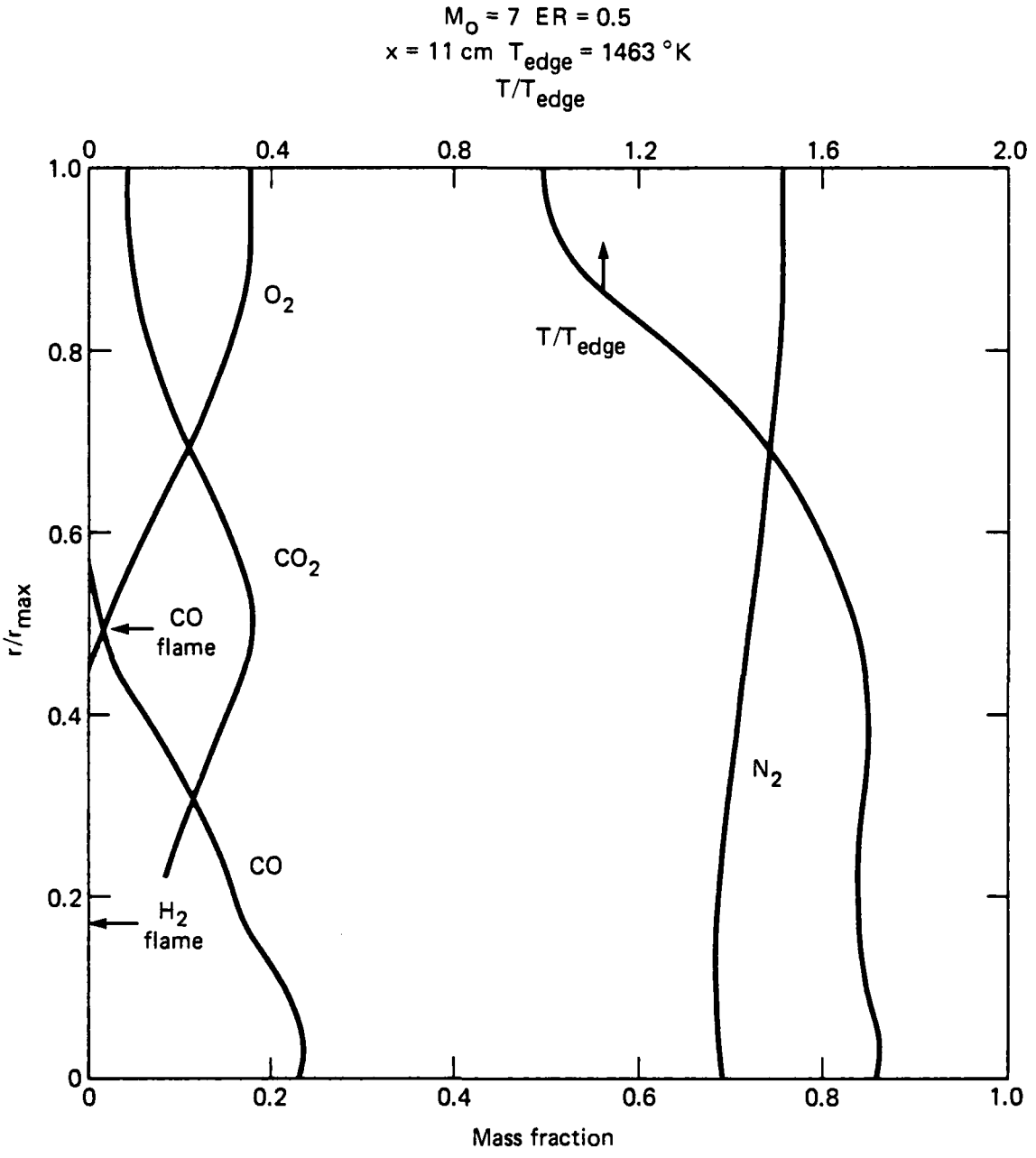

Fig. 23 Predicted profiles in flame region.

profiles at the combustor exit. Further details of this effort are given in Refs. 15, 30 and 31.

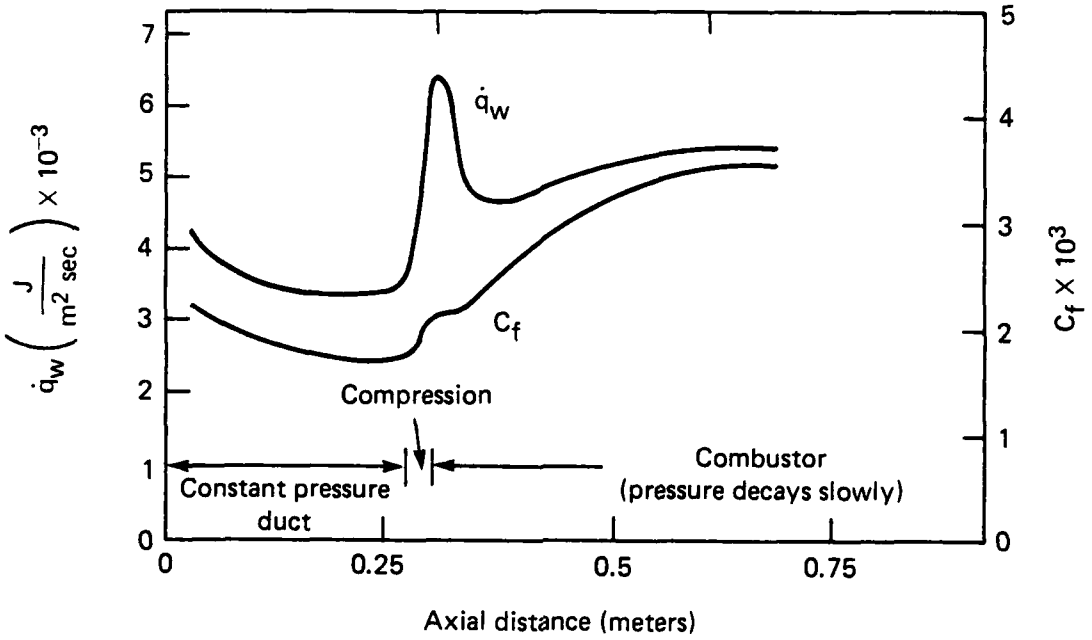

Fig. 24 Combustor wall skin friction coefficient and heat flux distributions for $M_0 = 7$ flight for ER = 0.5.

Calculations have been made for a typical scramjet nozzle case. The nozzle contour chosen for analysis is plotted in Fig. 26. The inlet flow to the nozzle was taken as the outlet flow from the mixing and burning code for

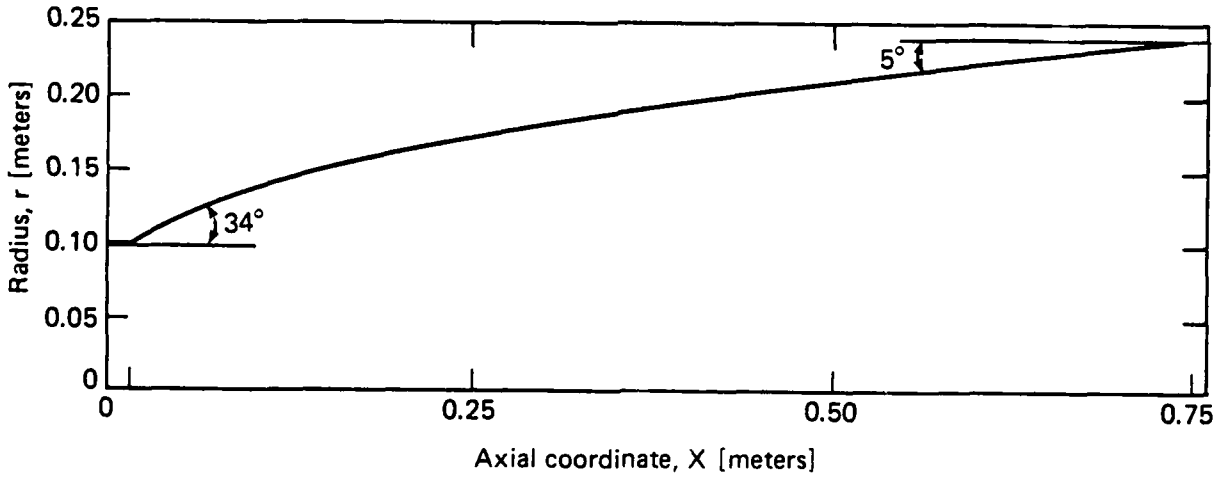

Fig. 26 Nozzle contour chosen for analysis.

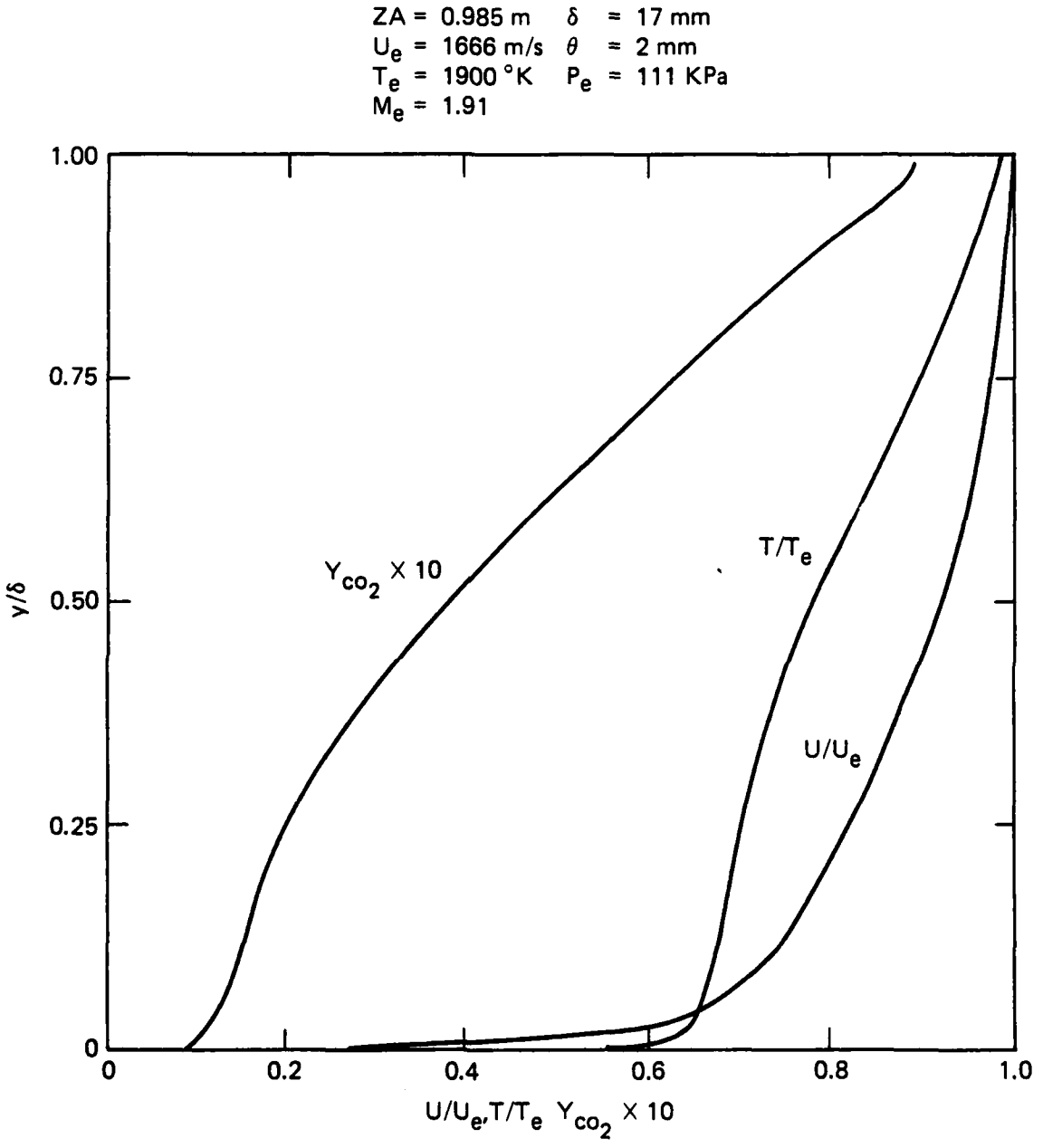

Fig. 25 Boundary layer profiles in DCR combustor exit plane at M_o = 7.

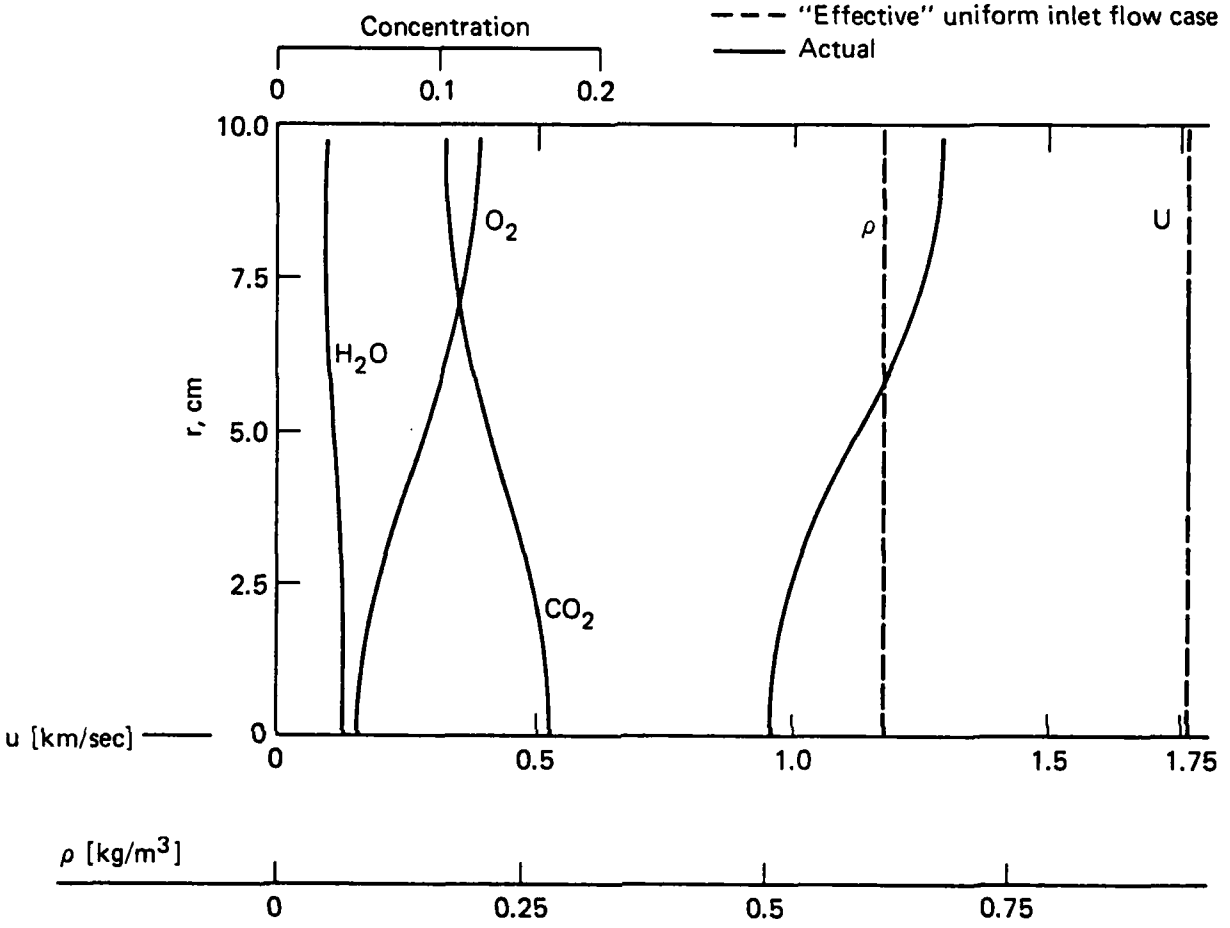

Fig. 27 Nozzle inlet profiles.

the combustor. The inlet property and species profiles are shown in Fig. 27. An "equivalent" all-air, uniform inlet flow case was constructed with the outer velocity and pressure from the nonuniform case and the same total mass flow. Some nozzle property exit profiles for the nonuniform and the associated uniform inlet profile cases are shown in Figs. 28 and 29 on p. 44-45, respectively.

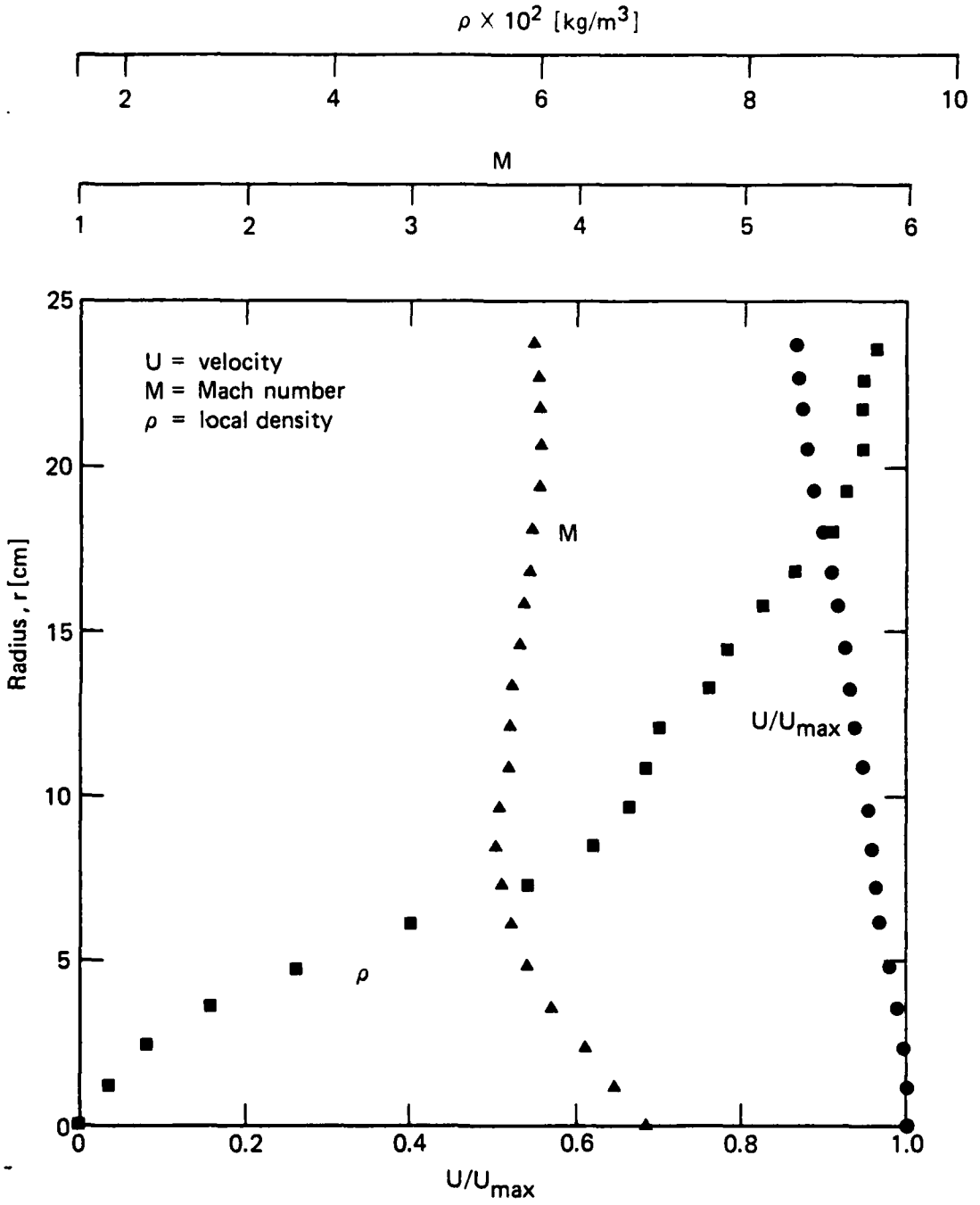

Fig. 28 Exit profiles - real, nonuniform inflow.

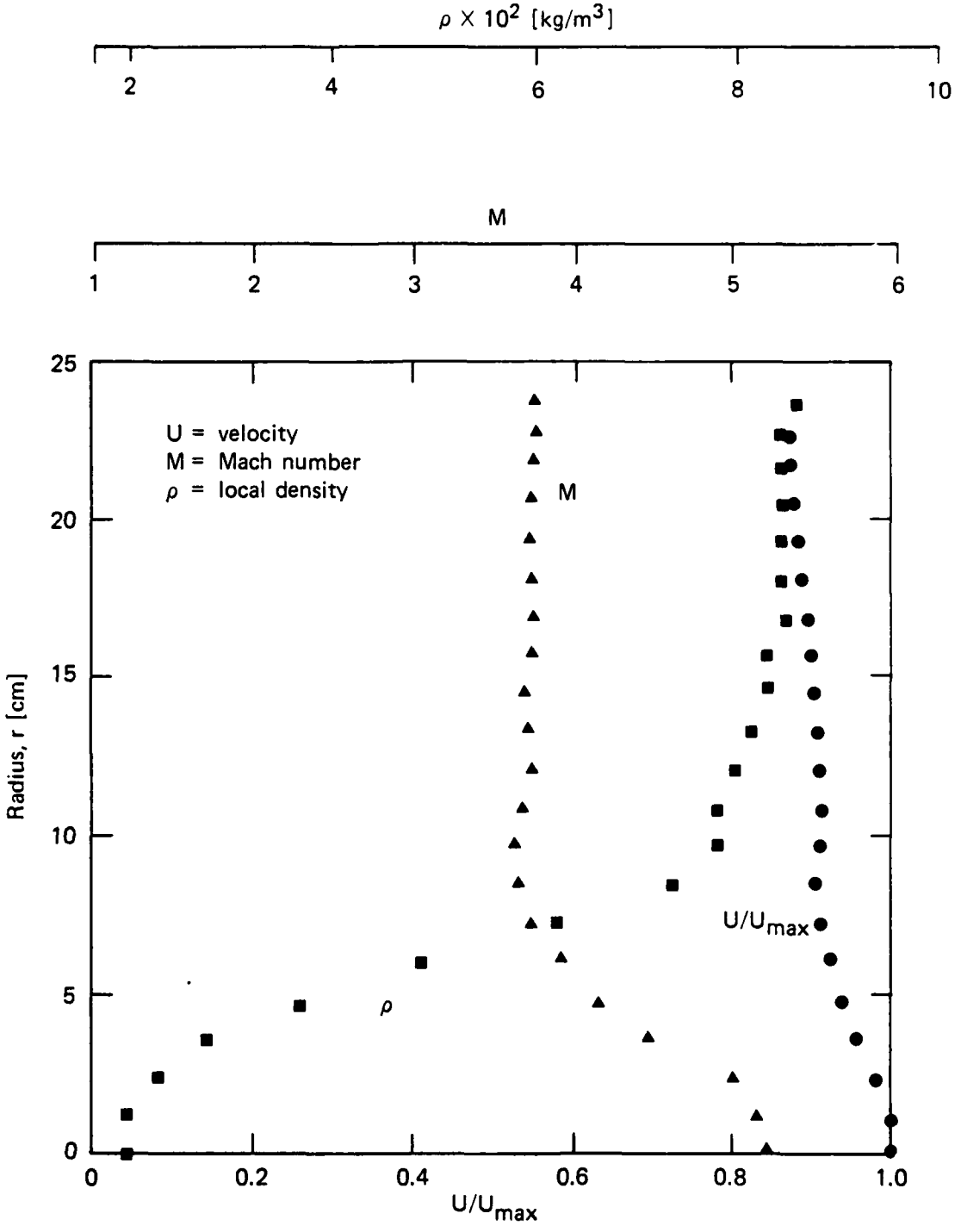

Fig. 29 Exit profiles - uniform inflow.

CONCLUSIONS AND RECOMMENDATIONS

Combustor/Inlet Interaction Tests

A procedure has been defined and tested for computing the instream flow properties in a ducted, supersonic flow where viscous effects are important. The only instream data required as input in this algorithm are the pitot pressures. The results are consistent with both theory and experimental data for similar flowfields. This consistency is with respect to the magnitude of both the mean (Ref. 2) and turbulent fluctuation components (Ref. 3) of the various flowfield properties of interest. Furthermore, this effort has shown that several alternate algorithms that model the instream static pressure, rather than the total pressure, were not as successful. Thus, the instream total pressure $p_t(r, z)$ is the best variable to model, and the model presented here for it is consistent with all pertinent physical constraints.

The experimental generation of the simulated precombustion compression field over the entire range of test variables has been demonstrated. The ducted compression field is generated by the expansion of compressed air to pressures that are considerably less than the ambient exhaust pressure. By varying the annulus plenum pressure over a narrow range, the shock structure in the annulus can be moved fore or aft, with the accompanying increase or decrease in the overall static pressure rise ratio. The generation of compression fields in the annular isolator duct with an ambient exhaust and with an overall pressure rise ratio greater than the normal shock value has been demonstrated at several different operating conditions.

Finally, a highly efficient interactive computer code has been developed to facilitate experimental data reduction. The computer graphics and other analytical features of this custom designed software permit one analyst to keep pace with a test schedule of up to 15 average runs per week. An average run involves the measurement and recording of about 200,000 data samples (and the corresponding 200,000 time samples) for about 250 locations in the flow. Static and/or total pressure and temperature are the data measured.

The experimental investigation is now armed with physical insight, analytical methods and data reduction codes needed for rapid and significant progress. The difficult period of grappling with unexpected experimental data, whose implications were unclear, is over. The experimental effort is in the production mode of operation, where the direction and objectives are clear and obtainable. Both the hardware and the software are fully tested and routinely operational. It is therefore recommended that the current rapid progress be sustained with continued funding.

Component and Engine Cycle Modeling

Computer codes have been developed to analyze (1) the recirculation region behind the gas generator base, (2) the coaxial mixing and burning in the supersonic combustor, (3) the combustor wall boundary layer, and (4) the nozzle flow. Base pressure predictions for Mach 2.03 and 2.30 freestream conditions have been completed. These calculations have included the effect of the upstream growth of the boundary layer momentum thickness on the base pressure. The coaxial mixing and burning code, using a two flame sheet model, has predicted that the H_2 and CO flames will be about 0.2 and 1.0 meters long, respectively, in the DCR combustor. Wall shear and heat transfer distributions in qualitative agreement with observed test results have been predicted. Finally, the numerical modeling of the ramjet nozzle flow has resulted in calculated nozzle exit profiles for the velocity, density and Mach number for both the simplified uniform nozzle inflow condition and for the real nonuniform entrance condition. The nonuniform entrance condition is specified by the radial variation of flowfield properties and chemical composition at the exit of the supersonic combustor, as predicted by the mixing and burning code. The accurate prediction of the nozzle flow is important because the net thrust developed by the engine is highly sensitive to the magnitude of the nozzle exit stream thrust whose value in turn depends on the finite rate chemical processes in the nozzle.

The component and engine cycle modeling effort has broken much new ground but has not yet synthesized all the modular analytical procedures. The two flame sheet coaxial mixing and burning code needs to be extended to treat multiple species. The inclusion of both finite rate and equilibrium chemistry

into the mixing and burning code needs to be completed. The preliminary analyses for the combustor wall shear and heat transfer need to be improved by replacing the initial simplifying assumptions with more sophisticated techniques. The analysis of the recirculation region of the gas generator base, a very complex and challenging problem, requires more analysis. The effect of the lip shock that follows the centered corner expansion could be included. The base flow analysis is very important because it produces the input data for the mixing and burning code, which produces the input data for all subsequent analytical modules. The extension of the VNAP2 code (from Los Alamos) for the numerical simulation of ramjet nozzle flows to handle varying chemical composition, to include additional species and to incorporate new procedures for calculating thermodynamic quantities should be completed. It is therefore recommended that the modeling program be continued in order to permit the synthesis and subsequent productive use of the various analytical tools thathave already been developed and to permit the continued refinement and improvement of these tools. In the final analysis, these recommendations will prove to be the least expensive path to fully develop a fundamental understanding and working knowledge of the flow processes in supersonic combustion ramjet engines.

REFERENCES

1. P. P. Pandolfini, P. J. Waltrup, et al., "Dual Combustion Ramjet Low Mach Number High Altitude Connected-Pipe Combustor Tests," presented at the 1984 JANNAF Conference, New Orleans, LA, 7-9 Feb. 1984.

2. R. D. Stockbridge, "Evaluation of the Mean Flow Properties and Boundary Layer Thicknesses in the Supersonic Annular Flowfield of the DCR Combustor/Inlet Interaction Tests," JHU/APL Quarterly Report, July-Sept. 1984.

3. R. D. Stockbridge, "Evaluation of the Turbulent Fluctuations in the Supersonic Annular Flowfield of the DCR Combustor/Inlet Interaction Tests," JHU/APL Quarterly Report, July-Sept. 1984.

4. P. J. Waltrup and F. S. Billig, "Structure of Shock Waves in Cylindrical Ducts," AIAA Journal 11, pp. 1404-1408, 1973.

5. H. H. Fernholz and P. J. Finley, A Critical Compilation of Compressible Turbulent Boundary Layer Data, NATO Advisory Group for Aerospace Research and Development, Agardograph No. 223 (June 1977).

6. A. L. Kistler, "Fluctuation Measurements in Supersonic Turbulent Boundary Layers," Ballistic Res. Lab. 1052 (1958) and Phys. Fluids 2 (1959).

7. P. J. Waltrup and J. A. Schetz, "An Experimental Investigation of a Compressible Turbulent Boundary Layer Subjected to a Systematic Variation of Adverse Pressure Gradients," Virginia Polytechnic Inst. VPI-E-71-18 (1971).

8. F. K. Owen, C. C. Horstman and M. L. Kussoy, "Mean and Fluctuating Flow Measurements of a Fully-Developed Non-Adiabatic Hypersonic Boundary Layer," J. Fluid Mech. 70, 393-413 (1975).

9. A. J. Laderman and A. Demetriades, "Mean and Fluctuating Flow Measurements in the Hypersonic Boundary Layer over a Cooled Wall," J. Fluid Mech. 63, 121-144 (1974).

10. F. S. Billig and G. L. Dugger, "The Interaction of Shock Waves and Heat Addition in the Design of Supersonic Combustors," Twelfth Symposium (International) on Combustion, The Combustion Institute, Pittsburgh, Pennsylvania, 1969, pp. 1125-1134.

11. J. A. Schetz and F. S. Billig, "Approximate Analysis of Base Burning in Supersonic Flow," Progress in Astronautics and Aerodynamics: Aerodynamics of Base Combustion, Vol. 40, edited by S.N.B. Murthy, AIAA, New York, 1976, pp. 385-405.

12. J. A. Schetz and F. S. Billig, "Simplified Analysis of Supersonic Base Flows Including Injection and Combustion," AIAA Journal, Vol. 14, January 1976, pp. 7-8.

13. J. A. Schetz, F. S. Billig and S. Favin, "Approximate Analysis of Axisymmetric Base Flows with Injection in Supersonic Flow," AIAA Journal, Vol. 18, August 1980, pp. 867-868.

14. J. A. Schetz, F. S. Billig and S. Favin, "Analysis of Base Drag Reduction by Base and/or External Burning," The Johns Hopkins University Applied Physics Laboratory, Laurel, Maryland, AIAA Journal, Vol. 19, No. 9, September 1981.

15. J. A. Schetz, F. S. Billig and S. Favin, "Analysis of Mixing and Combustion in a Scramjet Combustor with a Coaxial Fuel Jet," 16th AIAA/ASME/SAE Joint Propulsion Conference, AIAA Preprint 80-1256, June 1980.

16. J. A. Schetz and S. Favin, "Numerical Solution of the Near Wake of a Body with Propeller," J. of Hydronautics, Vol. 11, No. 4, October 1977, pp. 136-141.

17. J. A. Schetz, "A Simplified Model for the Combustion of Multicomponent Fuels in Air," Combustion and Flame, Vol. 15, No. 1, August 1970.

18. S. Gordon and B. McBride, "Computer Program for Calculation of Complex Equilibrium Compositions," NASA SP-273, 1971.

19. F. S. Billig, P. J. Waltrup and R. D. Stockbridge, "The Integral Rocket, Dual-Combustion Ramjet: A New Propulsion Concept," presented at the 4th International Symposium on Airbreathing Engines, ISABE/ICAS/AIAA, Lake Buena Vista, Florida, April 2-6, 1979, pp. 433-444.

20. J. A. Schetz, "Turbulent Mixing of a Jet in a Co-Flowing Stream," AIAA J., Vol. 6, October 1968, pp. 2008-2010.

21. L. Prandt, "Uber eine neues Formelsystem fur die ausgebildete Turbulenz," Nachrichten der Akad. Wiss., Gottingen, Mathphys., Van den Loeck & Ruprecht, Gottingen, 1945, pp. 6-19.

22. E. C. Anderson and C. H. Lewis, "Laminar or Turbulent Boundary Layer Flows of Perfect Gases or Reacting Gas Mixtures in Chemical Equilibrium," NASA CR-1893, October 1971.

23. R. H. Pletcher, "On a Calculation Method for Compressible Turbulent Boundary Flows with Heat Transfer," AIAA Paper 71-165.

24. F. G. Blottner, "Finite Difference Methods of Solution of the Boundary Layer Equations," AIAA Journal, February 1970.

25. R. A. Svehla and B. J. McBride, "FORTRAN IV Computer Program for Calculation of Thermodynamic and Transport Properties of Complex Chemical Systems," NASA TN D-7056, January 1973.

26. D. Coles, "Measurements of Turbulent Friction on a Smooth Flat Plate in Supersonic Flow," J. Aero. Sci., Vol. 21, No. 7, July 1954, pp. 433-448.

27. G. D. Huffman, D. R. Zimmerman and W. A. Bennett, "The Effect of Free-Stream Turbulent Level on Turbulent Boundary Layer Behavior," in AGARDograph No. 164, Boundary Layer Effects in Turbomechanics, December 1972.

28. F. S. Billig, J. A. Schetz and S. Favin, "A Simplified Technique for the Analysis of Base Flow Including the Effects of Lip Shock," Fifth International Symposium on Airbreathing Engines, Bangalore, India, February 16-22, 1981.

29. P. J. Waltrup, G. Y. Anderson (NASA), and F. D. Stull (AFAPL), "Supersonic Combustion Ramjet (Scramjet) Engine Development in the United States," invited papers presented at the 3rd International Symposium on Air Breathing Engines, Munich, Germany, March 1976, JHU/APL Preprint.

30. J. A. Schetz, F. S. Billig and S. Favin, "Scramjet Combustor Wall Boundary Layer Analysis," (U), AIAA/ASME/SAE 17th Joint Propulsion Conference, AIAA Preprint 81-1423, July 1981.

31. J. A. Schetz, F. S. Billig and S. Favin, "Flowfield Analysis of a Scramjet Combustor with a Coaxial Fuel Jet," AIAA Journal, Vol. 20, No. 9, September 1982, pp. 1268-1274.

NOMENCLATURE

A	= area
C_f	= skin friction coefficient
ER	= fuel-air equivalence ratio
h	= base height
k	= kinetic energy turbulence
ℓ	= length scale
M	= Mach number
p	= pressure
q_w	= wall heat flux
r	= radius
R	= body radius
Re	= Reynolds number
T	= temperature
u, v, w	= velocity components
w	= mass flow rate
x, z	= axial distance
y	= distance from wall
Y	= mass
ρ	= density
δ	= boundary layer thickness
δ^*	= boundary layer displacement thickness
δ_{KE}	= boundary layer kinetic energy thickness
Θ	= boundary layer momentum thickness
μ_T	= turbulent viscosity
ψ	= stream function

Subscripts

a	= supersonic annulus
e, edge	= edge condition
g	= gas generator
j	= jet
max	= maximum
o	= free stream (annulus)
t	= total
θ	= boundary layer momentum thickness

Superscripts

'	= pitot
-	= average quantity
~	= fluctuating quantity

END

FILMED

1-86

DTIC